QUANTUM SPECTROPOLARIMETRY AND THE SUN'S HIDDEN MAGNETISM

Javier Trujillo Bueno*

Instituto de Astrofísica de Canarias; 38205 La Laguna; Tenerife; Spain

ABSTRACT

Solar physicists can now proclaim with confidence that with the Zeeman effect and the available telescopes we can see only $\sim 1\%$ of the complex magnetism of the Sun. This is indeed regrettable because many of the key problems of solar and stellar physics, such as the magnetic coupling to the outer atmosphere and the coronal heating, will only be solved after deciphering how significant is the small-scale magnetic activity of the remaining $\sim 99\%$. The first part of this paper[1] presents a gentle introduction to *Quantum Spectropolarimetry*, emphasizing the importance of developing reliable diagnostic tools that take proper account of the Paschen-Back effect, scattering polarization and the Hanle effect. The second part of the article highlights how the application of quantum spectropolarimetry to solar physics has the potential to revolutionize our empirical understanding of the Sun's hidden magnetism.

Key words: Solar and Stellar Magnetic Fields, Spectropolarimetry, Level crossings and optical pumping.

1. INTRODUCTION

With the term "the Sun's hidden magnetism" I would like to refer to all those solar magnetic fields that with the available telescopes remain practically invisible to the Zeeman effect. The following examples belong to this category:

- $\sim 99\%$ of the magnetism of the 'quiet' solar photosphere.
- The solar chromosphere outside active regions.
- The dynamic jets that we call spicules.
- The magnetic fields that confine the plasma of solar prominences.
- The magnetism of the solar transition region and corona.

Unfortunately, our empirical knowledge of the Sun's hidden magnetism is still very primitive, especially concerning the outer solar atmosphere (chromosphere, transition region and corona). This is very regrettable because many of the physical challenges of solar and stellar physics arise precisely from magnetic processes taking place in such outer regions.

One option to improve the situation is to work hard to achieve a powerful (European?) ground-based solar facility optimized for high-resolution spectropolarimetric observations. Some relevant efforts are going into this direction, but we should also start thinking seriously on the enormous scientific interest of putting a high-sensitivity UV polarimeter in a solar space telescope (Trujillo Bueno et al. 2005*b*; see also Section 4.4). A second possibility is to try to create our own Sun in the computer, learning as much as possible from radiative magnetohydrodynamic numerical experiments. A third option is to give a chance to what I like to call *Quantum Spectropolarimetry*, that is, the possibility of diagnosing solar and stellar magnetic fields via the interpretation of spectral line polarization signals caused by a variety of unfamiliar physical processes, such as optical pumping, the Hanle effect, level-crossings and anti-level-crossings interferences, etc. Obviously, all three options should be pursued and cleverly combined to facilitate new advances in solar and stellar magnetism.

The emphasis of this keynote article is on the application of quantum spectropolarimetry to solar physics. The first part of the paper presents a 'gentle' introduction to this emerging field of research, emphasizing the importance of developing diagnostic tools that take proper account of the Zeeman and Paschen-Back effects, scattering polarization and the Hanle effect. Only in this way may we hope to investigate the strength and topology of stellar magnetic fields in a parameter domain which ranges

*Consejo Superior de Investigaciones Científicas (Spain)

[1]**Invited Review** at the 11^{th} European Solar Physics Meeting *The Dynamic Sun: Challenges for Theory and Observations* (ESA SP-600). Leuven (Belgium), 11–16 September 2005, Eds. D. Danesy, S. Poedts, A. De Groof & J. Andries. ESA Publications Division. Published on CDROM., p. 7.1, December 2005.

from field intensities as low as 1 milligauss to many thousands of gauss. The second part of the article shows some recent applications in solar physics with emphasis on the hidden magnetic fields of the photosphere, chromosphere and corona.

2. GENERATION OF POLARIZED RADIATION

It is suitable to begin by recalling that the state of polarization of a quasi-monochromatic beam of electromagnetic radiation can be conveniently characterized in terms of four quantities that can be measured by furnishing our telescopes with a polarimeter. Such observables are the four Stokes parameters (I, Q, U, V), which were formulated by Sir George Stokes in 1852 and introduced into astrophysics by the Nobel laureate Subrahmanyan Chandrasekhar in 1946. The Stokes $I(\lambda)$ profile represents the *intensity* as a function of wavelength, Stokes $Q(\lambda)$ the *intensity difference* between vertical and horizontal linear polarization, Stokes $U(\lambda)$ the *intensity difference* between linear polarization at $+45^\circ$ and -45°, while Stokes $V(\lambda)$ the *intensity difference* between right- and left-handed circular polarization (cf. Born & Wolf 1994). Note that the definition of the Stokes Q and U parameters requires first choosing a reference direction for $Q > 0$ in the plane perpendicular to the direction of propagation.

Let us now review the most important mechanisms that induce (and modify) polarization signatures in the spectral lines that originate in stellar atmospheres: the Zeeman and Paschen-Back effects, scattering processes and the Hanle effect.

2.1. The Zeeman effect

As illustrated in Figure 1, the Zeeman effect requires the presence of a magnetic field which causes the atomic and molecular energy levels to split into different magnetic sublevels characterized by their magnetic quantum number M (Condon & Shortley 1935). Each level of total angular momentum J splits into $(2J + 1)$ sublevels, the splitting being proportional to the level's Landé factor, g_J, and to the magnetic field strength. As a result, a spectral line between a lower level with (J_l, g_l) and an upper level with (J_u, g_u) is composed of several individual components whose frequencies are given by $\nu^{J_u M_u}_{J_l M_l} = \nu_0 + \nu_L(g_u M_u - g_l M_l)$, where ν_0 is the frequency of the line in the absence of magnetic fields and $\nu_L = 1.3996{\times}10^6 B$ is the Larmor frequency (with B the magnetic field strength expressed in gauss). In particular, a line transition with $J_l = 0$ and $J_u = 1$ has three components (see Fig. 1): one π component centered at ν_0 (or at λ_0), one $\sigma_{\rm red}$ component centered at $\nu_0 - g_u\nu_L$ (or at $\lambda_0 + g_u\Delta\lambda_B$), and one $\sigma_{\rm blue}$ component centered at $\nu_0 + g_u\nu_L$ (or at $\lambda_0 - g_u\Delta\lambda_B$), where $\Delta\lambda_B = 4.6686{\times}10^{-13}\lambda_0^2 B$ (with λ_0 in Å and B in gauss).

The important point to remember is that the polarization signals produced by the Zeeman effect are caused by the *wavelength shifts* between the π ($\Delta M = M_u - M_l = 0$) and $\sigma_{b,r}$ ($\Delta M = \pm 1$) transitions. Such wavelength shifts are also the physical origin of the spectral line polarization induced by the Paschen-Back effect discussed below in Section 2.5, since the only difference with respect to the *linear* Zeeman effect theory considered here lies in the calculation of the positions and strengths of the various π and σ components.

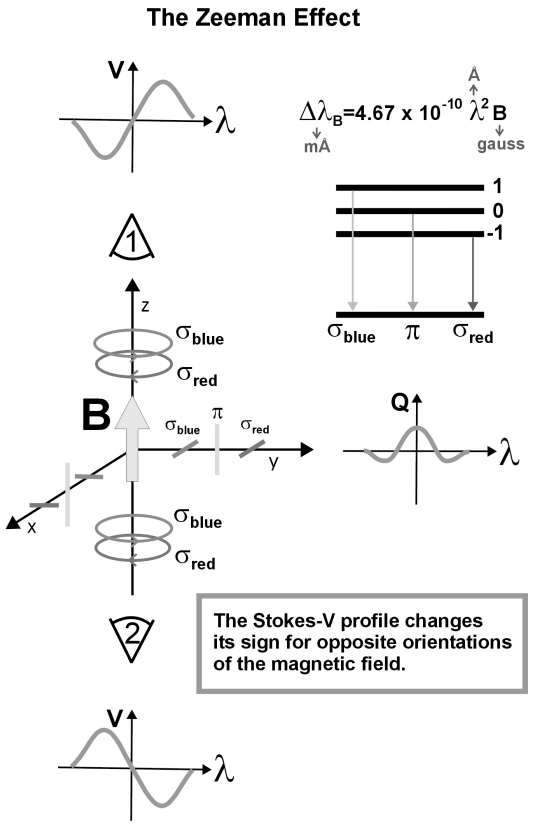

Figure 1. The oscillator model for the Zeeman effect indicating the characteristic shapes of the circular and linear polarization profiles as generated locally via the emission process. It is important to note that the Stokes $V(\lambda)$ profile changes its sign for opposite orientations of the magnetic field vector, while the Stokes $Q(\lambda)$ profile reverses sign when the transverse field component is rotated by $\pm 90^\circ$.

The Zeeman effect is most sensitive in *circular* polarization (quantified by the Stokes V parameter), with a magnitude that for not too strong fields scales with the ratio between the Zeeman splitting and the width of the spectral line (which is very much larger than the natural width of the atomic levels!), and in such a way that the emergent Stokes $V(\lambda)$ profile changes its sign for opposite orientations of the magnetic field vector. This so-called *longitudinal* Zeeman effect responds to the line-of-sight component of the magnetic field. Accordingly, if

we have a perfect cancellation of mixed magnetic polarities within the spatio-temporal resolution element of the observation, the measured circular polarization would be exactly zero *if* the thermodynamic and dynamic properties of the mixed magnetic components are similar. The antisymmetric shape of the Stokes $V(\lambda)$ profiles illustrated in Fig. 1 can be easily understood by noting the expression of the Stokes-V component of the emission vector:

$$\epsilon_V = \frac{h\nu}{4\pi} N_u A_{ul} \frac{1}{2} [\phi_{\rm red} - \phi_{\rm blue}] \cos\theta, \qquad (1)$$

where θ is the angle between the magnetic field vector and the line of sight, A_{ul} the Einstein coefficient for the spontaneous emission process, N_u the number of atoms per unit volume in the upper level of the line transition under consideration, while $\phi_{\rm red}$ and $\phi_{\rm blue}$ are profiles that result from the superposition of the Voigt functions corresponding to each individual component. $\phi_{\rm red}$ is displaced to the red side of the central wavelength λ_0, and $\phi_{\rm blue}$ to the blue side. For instance, for the particular case of a line transition with $J_l = 0$ and $J_u = 1$, $\phi_{\rm red}$ is a Voigt profile centered at $\lambda_0 + g_u \Delta\lambda_B$ and $\phi_{\rm blue}$ a Voigt profile centered at $\lambda_0 - g_u \Delta\lambda_B$.

In contrast, the *transverse* Zeeman effect responds to the component of the magnetic field perpendicular to the line of sight, but produces *linear* polarization signals (quantified by the Stokes Q and U parameters) that are normally below the noise level of present observational possibilities for intrinsically weak fields (typically B < 100 gauss for solar spectropolarimetry). The Stokes Q and U profiles induced by the Zeeman effect at a given point in a magnetized plasma have a three-lobe shape which is also illustrated in Fig. 1. This characteristic shape can be easily understood by noting that the expression of the Stokes-Q component of the emission vector is:

$$\epsilon_Q = \frac{h\nu}{4\pi} N_u A_{ul} \frac{1}{2} [\phi_\pi - (\frac{\phi_{\rm red} + \phi_{\rm blue}}{2})] \sin^2\theta \cos 2\chi, \qquad (2)$$

where χ is the angle that the projection line of the magnetic field vector on the plane perpendicular to the direction of propagation forms with the reference direction chosen for $Q > 0$.

Figure 2 shows an interesting example of Stokes profiles produced by the solar atmospheric plasma. The top panel is a section of the Fraunhofer spectrum between 4602 Å and 4610 Å showing the familiar absorption lines corresponding to several chemical elements. The remaining panels give the fractional polarizations $X(\lambda)/I(\lambda)$ (with $X = Q, U, V$). The spectrograph slit was placed parallel to and 2.5 arcsec inside the limb (at $\mu = 0.07$, where μ is the cosine of the heliocentric angle), such that half of the slit covers a significantly magnetized region, while the other half lies outside it. In the magnetically active region (which corresponds to the lower half of each of the four panels of Fig. 2) we see the characteristic signatures of the Zeeman effect. The V/I panel shows the typical

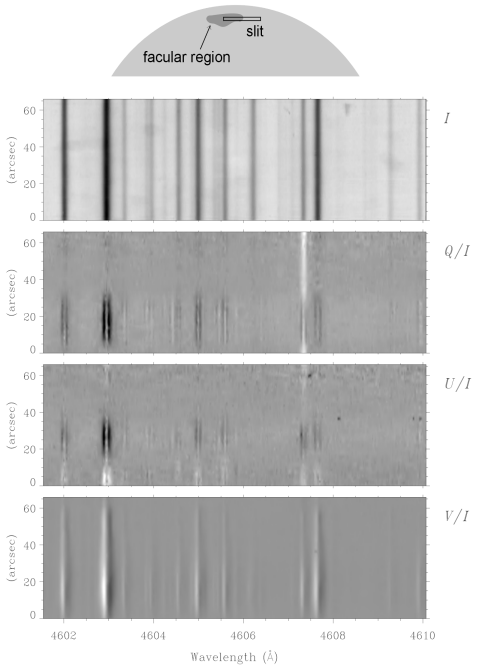

Figure 2. Spectropolarimetric observation close to the edge of the solar disk with half of the spectrograph slit crossing a moderately magnetized facular region. Note that while the characteristic signature of the longitudinal Zeeman effect is present at all spatial points along the slit, the signature of the transverse Zeeman effect disappears as soon as one goes outside the facular region. Interestingly, the only spectral line which shows linear polarization outside the facular region is the Sr I *line at* 4607 *Å with a* Q/I *shape that has nothing to do with the transverse Zeeman effect. This spectropolarimetric observation was obtained by Stenflo (2002).*

antisymmetric signature of the longitudinal Zeeman effect with a positive and a negative lobe for each spectral line, while in the lower half of the panels for Q/I and U/I we see the typical symmetric signature of the transverse Zeeman effect with two lobes in the wings of opposite sign to the central lobe. Interestingly, as soon as we go outside the facular region (see the upper half of each of the four panels in Fig. 2) we see that the amplitude of the circular polarization is significantly reduced in all atomic lines, while practically the only existing linear polarization signal is the Q/I peak corresponding to the Sr I line at 4607 Å . However, the shape of this Q/I profile is Gaussian-like, suggesting that it is not produced by the transverse Zeeman effect. If it does not result from the Zeeman effect, what, then, could its physical origin be?

2.2. Atomic level polarization

The amplitudes of polarization signals induced by the Zeeman effect are very small when the Zeeman splitting is a very small fraction of the spectral line width. If there

is no Zeeman splitting, there is no wavelength shift between the π and σ transitions, and there is no measurable polarization because the polarizations of such components cancel out. However, it is easy to see that this is only true if the populations of the magnetic sublevels pertaining to the lower and/or upper levels of the spectral line under consideration are assumed to be identical.

To this end, consider the case of a line transition with $J_l = 0$ and $J_u = 1$ and choose the quantization axis of total angular momentum along the solar radius vector through the observed point. Assume that the population of the upper-level magnetic sublevel with $M_u = 0$ is *smaller* than the populations of the magnetic sublevels with $M_u = \pm 1$. As a result, even in the absence of a magnetic field (zero Zeeman splitting), we can have a non-zero linear polarization signal, simply because the number of σ transitions per unit volume and time will be larger than the ensuing number of π transitions. Thus, a more general expression for the Stokes-Q component of the emission vector would be the following[2]

$$\epsilon_Q = \frac{h\nu}{4\pi} 3A_{ul} \frac{1}{2} [\, \rho_1(0,0)\phi_\pi - \qquad (3)$$

$$- \left(\frac{\rho_1(-1,-1)\phi_{\rm red} + \rho_1(1,1)\phi_{\rm blue}}{2} \right)] \sin^2\theta,$$

where θ is the angle between the quantization axis of total angular momentum (chosen here along the solar radius vector through the observed point) and the line of sight, while $\rho_{J_u}(M,M)$ is the population of the upper-level sublevel with magnetic quantum number M. This expression shows clearly that in the absence of a magnetic field (i.e., when $\phi_\pi = \phi_{\rm red} = \phi_{\rm blue}$ because their central wavelengths coincide at λ_0 for $B = 0$ gauss) the Stokes-Q profile is equal to the difference between two Voigt profiles: one (resulting from the π transition) centered at λ_0 and an extra one (resulting from the σ transitions) centered also at λ_0 but of *greater* amplitude. This is precisely the explanation of the curious linear polarization of the Sr I line seen Fig. 2, as observed in "quiet" regions close to the edge of the solar disk. Given that this spectral line has $J_l = 0$, its linear polarization is totally due to the *selective emission* processes resulting from the population imbalances of the upper level.

On the other hand, it is very important to understand that whenever the Zeeman splitting is a very small fraction of the spectral line width, spectral lines with $J_l = 1$ and $J_u = 0$ can produce linear polarization *only* if there exist population imbalances among the magnetic sublevels of their *lower-level*. If this is the case, then linear polarization can be generated via the *selective absorption* resulting from the population imbalances of the lower level (Trujillo Bueno & Landi Degl'Innocenti 1997; Trujillo Bueno 1999, 2001, 2003*a*; Trujillo Bueno et al. 2002*a*). The same applies to $J_l = 3/2 \rightarrow J_u = 1/2$ transitions, like the $\lambda 8662$ Å line of the Ca II IR triplet (Manso Sainz & Trujillo Bueno 2003). Interestingly, lower-level atomic polarization and the ensuing selective absorption mechanism (i.e., 'zero-field' dichroism) is the physical origin of the 'enigmatic' signals of the linearly-polarized solar limb spectrum (or *second solar spectrum*) which has been discovered recently using novel polarimeters that allow the detection of very low amplitude polarization signals (with $10^{-6} < Q/I < 10^{-3}$; see Stenflo & Keller 1997; Stenflo et al. 2000; Gandorfer 2000, 2002, 2005).

In summary, spectral line polarization can be produced by the mere presence of *atomic level polarization*, i.e., by the existence of population imbalances among the sublevels pertaining to the upper and/or lower atomic levels involved in the line transition under consideration.[3] Upper-level polarization imply *sources* of polarization (through the emission process), while lower-level polarization produce *sinks* of polarization (through the absorption process).

2.3. Anisotropic radiation pumping

What is the key physical mechanism that induces atomic level polarization in a stellar atmosphere? The answer lies in the *the anisotropic illumination of the atoms*. This is easy to understand by considering the academic case of a unidirectional unpolarized light beam that illuminates a gas of two-level atoms with $J_l = 0$ and $J_u = 1$ and that is propagating along the direction chosen as the quantization axis of total angular momentum. Since these atoms can only absorb ± 1 units of angular momentum from the light beam, only transitions corresponding to $\Delta M = \pm 1$ are effective, so that no transitions occur to the $M = 0$ sublevel of the upper level. Thus, in the absence of any relaxation mechanisms, the upper-level sublevels with $M = 1$ and $M = -1$ would be more populated than the $M = 0$ sublevel and the *alignment coefficient* $\rho^2_0(J_u = 1) = (N_1 - 2N_0 + N_{-1})/\sqrt{6}$ would have a positive value.

Upper-level selective population pumping occurs when some *upper state* sublevels have more chance of being populated than others. On the contrary, as illustrated in Fig. 3, lower-level selective depopulation pumping occurs when some *lower state* sublevels absorb light more strongly than others. As a result, an excess population tends to build up in the weakly absorbing sublevels (Kastler 1950; Happer 1972; Trujillo Bueno & Landi Degl'Innocenti 1997; Trujillo Bueno 1999, 2001; Trujillo Bueno et al. 2002*a*; Manso Sainz & Trujillo Bueno 2003). It is also important to note that line transitions between levels having other total angular momentum values (e.g., $J_l = J_u = 1$) permit the transfer of atomic polarization between both levels via a process called *repopulation pumping* (e.g., lower-level atomic polarization can result simply from the spontaneous decay of a *polarized* upper level). The presence of a magnetic field

[2] I have chosen here the positive reference direction for $Q > 0$ such that $\cos 2\chi = 1$.

[3] As we shall see below while introducing the Hanle effect, the concept of *atomic polarization* includes also the possibility of quantum interferences (or coherences) among the magnetic sublevels of each J-level, and even among those belonging to different J-levels.

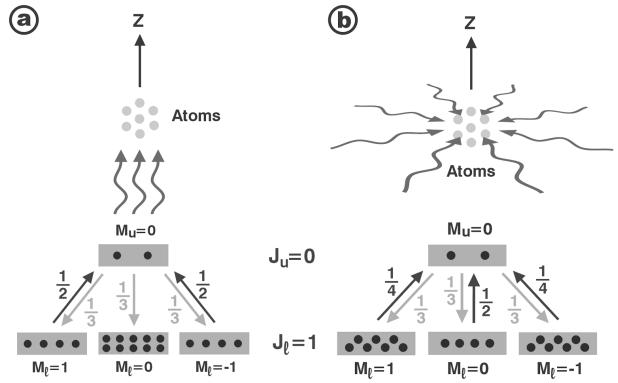

Figure 3. Illustration of the atomic polarization that is induced in the lower level of a two-level atom (with $J_l = 1$ and $J_u = 0$) by two types of anisotropic illuminations ($\mathbf{a}$ and $\mathbf{b}$). The incident radiation field is assumed to be unpolarized and with axial symmetry around the vertical direction, which is our choice here for the quantization axis of total angular momentum. In both cases, an excess population tends to build up in the weakly absorbing sublevels. Note that the alignment coefficient of the lower level (i.e. $\rho^2_0 = (N_1 - 2N_0 + N_{-1})/\sqrt{6}$, N_i being the populations of the magnetic sublevels) is negative in case $(\mathbf{a})$ (where the incident beam is parallel to the quantization axis), but positive in case $(\mathbf{b})$ (where the incident beams are perpendicular to the quantization axis). The physical understanding of the information provided in this figure is left as an exercise to the reader.

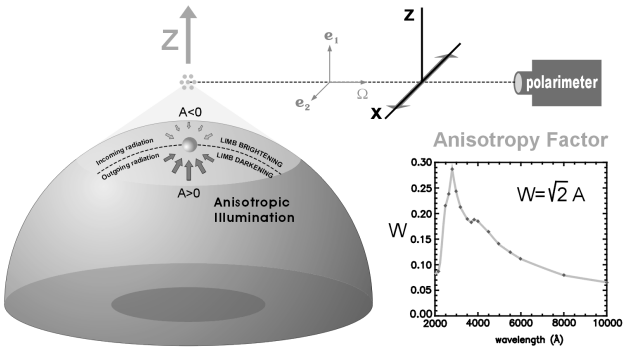

Figure 4. Anisotropic illumination of the outer layers of a stellar atmosphere, indicating that the outgoing continuum radiation shows limb darkening while the incoming radiation shows limb brightening. The 'degree of anisotropy' of the incident radiation field is quantified by $A = J^2_0/J^0_0$, where J^0_0 is the familiar mean intensity and $J^2_0 \approx \oint \frac{\mathrm{d}\vec{\Omega}}{4\pi} \frac{1}{2\sqrt{2}}(3\mu^2 - 1) I_{\nu,\vec{\Omega}}$ (with $I_{\nu,\vec{\Omega}}$ the Stokes-I parameter as a function of frequency ν and direction $\vec{\Omega}$, while $\mu = \cos\theta$, with θ the polar angle with respect to the Z-axis). The possible values of the 'anisotropy factor' $\mathrm{W} = \sqrt{2}\,A$ vary between $\mathrm{W} = -1/2$, for the limiting case of illumination by a purely horizontal radiation field without any azimuthal dependence (case b of Fig. 3), and $\mathrm{W} = 1$ for purely vertical illumination (case a of Fig. 3). It is important to point out that the larger the 'anisotropy factor' the larger the fractional atomic polarization that can be induced, and the larger the amplitude of the emergent linear polarization. We choose the positive direction for the Stokes-Q parameter along the X-axis, i.e. along the perpendicular direction to the stellar radius vector through the observed point. The inset shows the wavelength dependence of the anisotropy factor corresponding to the center to limb variation of the observed solar continuum radiation.

is not necessary for the operation of such optical pumping processes, which can be particularly efficient in creating atomic polarization if the depolarizing rates from elastic collisions are sufficiently low. Figure 4 illustrates the type of anisotropic illumination in the outer layers of a stellar atmosphere.

2.4. The Hanle effect

The Hanle effect is the modification of the atomic-level polarization (and of the ensuing observable effects on the emergent Stokes profiles Q and U) caused by the action of a magnetic field *inclined* with respect to the symmetry axis of the pumping radiation field. The basic formula to estimate the magnetic field intensity, $B_{\rm H}$ (measured in gauss), sufficient to produce a sizable change in the atomic level polarization results from equating the Zeeman splitting with the natural width (or inverse lifetime) of the energy level under consideration:

$$2\pi\nu_L\, g_J \;=\; 8.79{\times}10^6\; B_{\rm H}\; g_J \;\approx\; 1/t_{\rm life}\;, \qquad (4)$$

where ν_L is the Larmor frequency, while g_J and $t_{\rm life}$ are, respectively, the Landé factor and the level's lifetime (in seconds), which can be either the upper or the lower level of the chosen spectral line. The application of this basic formula to the upper and lower levels of typical spectral lines shows that the Hanle effect may allow us to diagnose stellar magnetic fields having intensities between milligauss and a few hundred gauss, i.e., in a parameter domain that is very hard to study via the Zeeman effect alone.

Figure 1 of Trujillo Bueno (2001) illustrates the oscillator model for the Hanle effect including a detailed classical description of the influence of a weak magnetic field on the linear polarization caused by scattering processes (see also Hanle 1924, Mitchell & Zemansky 1934, Stenflo 1994, Landi Degl'Innocenti & Landolfi 2004). In order to point out that depending on the scattering geometry, the Hanle effect can either destroy or create linear polarization in spectral lines, let us consider scattering processes in a $J_l = 0 \rightarrow J_u = 1$ line transition for the following two geometries: 90° scattering and forward scattering.

(a) 90° **scattering**

Figure 5 illustrates the 90° scattering case, in the absence and in the presence of a magnetic field. For this geometry the largest polarization amplitude occurs for the zero field reference case, with the direction of the linear polarization as indicated in the top panel (i.e, perpendicular to the scattering plane).

The two lower panels illustrate what happens when the scattering processes take place in the presence of a magnetic field pointing (a) towards the observer (left panel) or (b) away from him/her (right panel). In both situations the polarization amplitude is *reduced* with respect to the previously discussed unmagnetized case. Moreover, the direction of the linear polarization is *rotated* with respect to the zero field case. Typically, this rotation is *counterclockwise* for case (a), but *clockwise* for case (b)[4]. Therefore, when opposite magnetic polarities coexist within the spatio-temporal resolution element of the observation the direction of the linear polarization is like in the top panel of Fig. 5, simply because the rotation effect cancels out. However, the polarization amplitude is indeed reduced with respect to the zero field reference case, which provides an "observable" that can be used for obtaining empirical information on hidden, mixed polarity fields at subresolution scales in the solar atmosphere (Stenflo 1982; Trujillo Bueno et al. 2004).

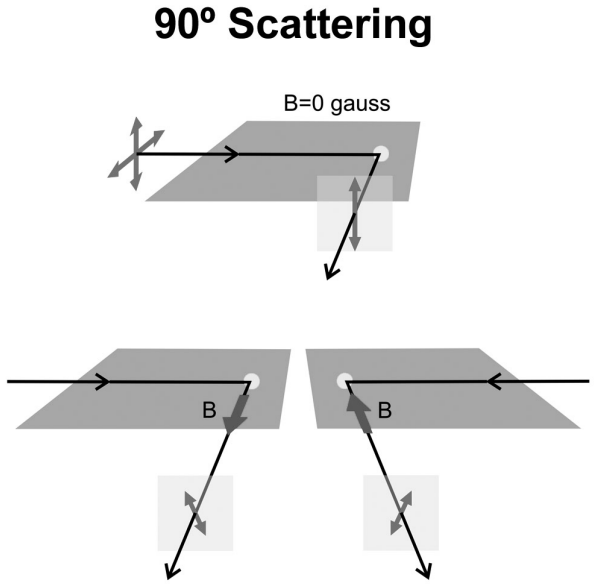

Figure 5. The 90° scattering case in the absence (top panel) and in the presence (bottom panels) of a deterministic magnetic field.

(b) Forward scattering

Figure 6 illustrates the case of forward scattering, in the absence and in the presence of a magnetic field. In this geometry we have *zero* polarization for the unmagnetized reference case, while the largest linear polarization (oriented along the direction of the external magnetic field) is found for "sufficiently strong" fields (i.e., for a magnetic strength such that the ensuing Zeeman splitting is much larger than the level's natural width).

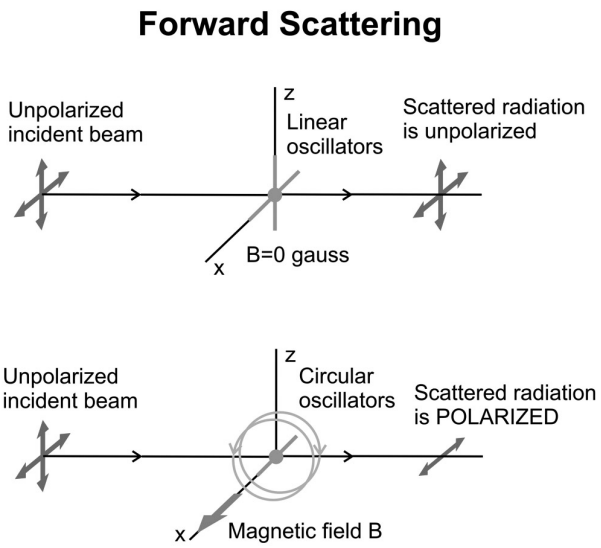

Figure 6. The forward scattering case, in the absence (top panel) and in the presence (bottom panel) of a deterministic magnetic field.

In other words, in the presence of an *inclined* magnetic field that breaks the symmetry of the scattering polarization problem, forward scattering processes can produce linear polarization signals in spectral lines. In this case, the linear polarization is *created* by the Hanle effect, a physical phenomenon that has been clearly demonstrated via spectropolarimetry of solar coronal filaments in the He I 10830 Å multiplet (Trujillo Bueno et al. 2002a).

The He I 10830 Å multiplet originates between a lower term (2^3S_1) and an upper term ($2^3P_{2,1,0}$). Therefore, it comprises three spectral lines: a 'blue' component at 10829.09 Å (with $J_l = 1$ and $J_u = 0$), and two 'red' components at 10830.25 Å (with $J_u = 1$) and at 10830.34 Å with ($J_u = 2$) which appear blended at solar atmospheric temperatures. It is important to point out that the upper level of the 'blue' line cannot carry any atomic polarization because its total angular momentum is $J_u = 0$. Therefore, whenever the Zeeman splitting is a very small fraction of the spectral line width, the only mechanism capable of producing linear polarization in the blue line is the *selective absorption* that results from the population imbalances of the lower level with $J_l = 1$. However, linear polarization in the 'red' line can be produced by both *selective emission* and *selective absorption*. Figure 7 shows an illustrative example of the creation of linear polarization signals by the Hanle effect in forward scattering at the solar disk center. Observations of this type of forward scattering polarization signals can be seen in Trujillo Bueno et al. (2002a), Collados et al. (2003) and Lagg et al. (2004).

[4]This occurs when the Landé factor, g_L, of the transition's upper level is positive, while the opposite behavior takes place if $g_L < 0$.

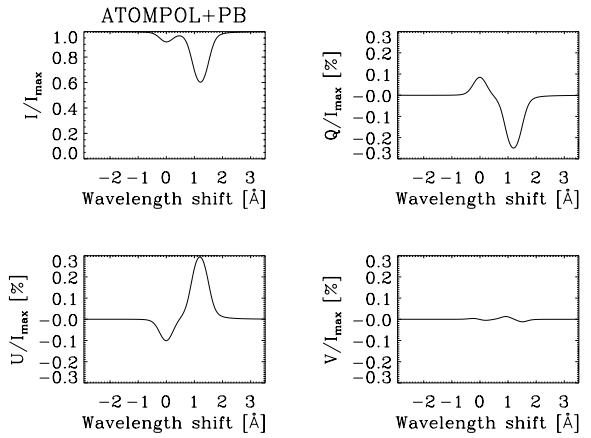

Figure 7. Model calculation of the emergent Stokes profiles of the He I *10830 Å multiplet at $\mu = 1$ assuming that a slab of helium atoms at a height of 3 arcseconds in the solar atmosphere is permeated by a deterministic magnetic field of 25 G with inclination $\theta_B = 85°$ and azimuth $\chi_B = 65°$. While the Stokes V profile is caused by the longitudinal Zeeman effect, the linear polarization profiles are entirely due the Hanle effect in forward scattering. We note that if the horizontal component of the magnetic field vector had been chosen parallel to the positive reference direction for Stokes Q (i.e., $\chi_B = 0°$), then $U = 0$ and $Q < 0$ in the 'blue' line and $Q > 0$ in the 'red' line.*

As seen in Figs. 5 and 6, the classical description of the Hanle effect is relatively easy to understand (cf., Trujillo Bueno 2001; Landi Degl'Innocenti & Landolfi 2004). In what follows, I provide a very brief explanation within the framework of quantum mechanics, since this is required for a deeper physical understanding of this fascinating effect which has found so many interesting applications in physics (see Moruzzi & Strumia 1991).

To that end, we need to recall first the concept of quantum coherence ($\rho_J(M, M')$) between different magnetic sublevels M and M' pertaining to each J-level. We say that the quantum coherence $\rho_J(M, M')$ is non-zero when the wave function presents a well defined phase relationship between the pure quantum states $|JM\rangle$ and $|JM'\rangle$. It is actually very common to find non-zero coherences while describing the excitation state of an atomic or molecular system under the influence of a pumping radiation field. Let us again consider a two-level atom with $J_l = 0$ and $J_u = 1$ that is being irradiated by an *unpolarized* radiation beam. In the absence of magnetic fields, all coherences of the upper level are zero *if* the quantization axis of total angular momentum is chosen along the symmetry axis of the pumping radiation beam. The same happens if a magnetic field is aligned with the quantization axis and this axis coincides with the symmetry axis of the radiation field that 'illuminates' the atomic system. This is because unpolarized radiation propagating along the quantization axis can only produce *incoherent* excitation of the upper-level sublevels with $M = \pm 1$.[5] If we now rotate the original reference system so that the new quantization axis for total angular momentum forms a non-zero angle with the symmetry axis of the radiation field, then non-zero coherences arise in this new reference system, even in the absence of a magnetic field. As shown below in Eq. (5), a magnetic field will *relax* such quantum coherences.

We thus see that the most general description of the excitation state of a J-level requires $(2J+1)^2$ quantities: the individual populations ($\rho_J(M, M)$) of the $(2J+1)$ sublevels and the degree of quantum coherence between each pair of them ($\rho_J(M, M')$). These quantities are nothing but the diagonal and non-diagonal elements of the *atomic density matrix* associated with the J-level, as given by the standard representation. Alternatively, we can use the multipole components (ρ^K_Q) of the atomic density matrix, which are given by linear combinations of $\rho_J(M, M')$. The ρ^K_Q elements with $Q = 0$ are *real* numbers given by linear combinations of the populations of the various Zeeman sublevels corresponding to the level of total angular momentum J. The total population of the atomic level J is proportional to $\sqrt{2J+1}\rho^0_0(J)$, while the population imbalances among the Zeeman sublevels are quantified by ρ^K_0 (e.g., $\rho^2_0(J = 1) = (N_1 - 2N_0 + N_{-1})/\sqrt{6}$ and $\rho^1_0(J = 1) = (N_1 - N_{-1})/\sqrt{2}$). However, the ρ^K_Q elements with $Q \neq 0$ are *complex* numbers given by linear combinations of the *coherences* between Zeeman sublevels whose magnetic quantum numbers differ by Q (e.g., $\rho^2_2(J = 1) = \rho(1, -1)$). These multipole components of the atomic density matrix provide the most useful way of quantifying, at the atomic level, the information we need for calculating the *sources* and *sinks* of polarization. Thus, the ρ^0_0 elements produce the dominant contribution to the Stokes I parameter, the ρ^1_Q elements (the *orientation* components) affect the circular polarization, while the ρ^2_Q elements (the *alignment* components) contribute to the *linear* polarization signals.

The Hanle effect can be suitably summarized by the following equation (Landi Degl'Innocenti & Landolfi 2004):

$$\rho^K_Q(J_u) = \frac{1}{1 + iQ\Gamma_u}[\rho^K_Q(J_u)]_{B=0}, \qquad (5)$$

where $\Gamma_u = 8.79\times10^6\ B\ g_{J_u}/A_{ul}$ and $[\rho^K_Q(J_u)]_{B=0}$ are the ρ^K_Q elements for the non-magnetic case defined in the reference frame in which the quantization axis is aligned with the magnetic field vector. This equation shows clearly that *in the magnetic field reference frame* the population imbalances (i.e., the ρ^K_Q elements with $Q = 0$) are unaffected by the magnetic field, while the ρ^K_Q elements with $Q \neq 0$ are *reduced* and *dephased* with respect to the non-magnetic case. The important point to remember is that the Hanle effect modifies the emergent Stokes Q and U profiles because the polarization

[5] Note that an unpolarized radiation beam may be considered as the incoherent superposition of right-handed and left-handed circular polarization.

of the light that is emitted and/or absorbed at each point within the astrophysical plasma under consideration depends sensitively on the local values of the ρ^K_Q elements along the line of sight.

Finally, it is interesting to mention that the Hanle effect played a fundamental role in the development of quantum mechanics because it led to the introduction and clarification of the concept of *coherent superposition* of pure states (Bohr 1924; Heisenberg 1925). As we have hinted above, the Hanle effect is directly related to the generation of coherent superposition of degenerate Zeeman sublevels of an atom (or molecule) by a light beam.[6] As the Zeeman sublevels are split by the magnetic field, the degeneracy is lifted and the coherences are modified. This gives rise to a characteristic magnetic-field dependence of the linear polarization of the scattered light that is finding increasing application as a diagnostic tool for magnetic fields in astrophysics (e.g., Asensio Ramos et al. 2005).

2.5. The Paschen-Back effect

As mentioned in Section 2.1, any atomic level of total angular momentum quantum number J is split by the action of a magnetic field into $(2J+1)$ *equally spaced* sublevels, the splitting being proportional to the Landé factor g_J and to the magnetic field strength. This well-known result of first-order perturbation theory is correct only if the splitting produced by the magnetic field on a $J-$level is small compared to the energy separation between the different $J-$levels of the (L,S) term under consideration. In other words, the standard theory of the Zeeman effect is valid only in the limit of "weak" magnetic fields. Here, "weak" means that the coupling of either the spin or the orbital angular momentum to the magnetic field is *weaker* than the coupling between the spin and the orbital angular momentum (the spin-orbit coupling). This is the so-called *Zeeman effect regime*.

In the opposite limit, the magnetic field is so "strong" that the spin-orbit interaction can be considered as a perturbation compared to the magnetic interaction. In this case the magnetic field dissolves the fine structure coupling – that is, $\vec{L}$ and $\vec{S}$ are practically decoupled and precess independently around $\vec{B}$. Therefore, the quantum number J loses its meaning. In this so-called *complete Paschen-Back effect regime* the magnetic Hamiltonian is diagonal on the basis $|LSM_LM_S\rangle$, and the term (L,S) splits into a number of components, each of which corresponds to particular values of (M_L+2M_S).

Interestingly, since the spin-orbit coupling increases rapidly with increasing nuclear charge, the conditions for a "strong" field are met at a much lower field with light atoms (like helium) than with heavy atoms. For instance, the levels with $J=2$ and $J=1$ of the upper term 2^3P of the He I 10830 Å multiplet cross for magnetic strengths between 400 G and 1500 G, approximately. This level-crossing regime corresponds to the *incomplete Paschen-Back effect regime*, in which the energy eigenvectors are gradually evolving from the form $|LSJM\rangle$ to the form $|LSM_LM_S\rangle$ as the magnetic field increases. This range between the limiting cases of "weak" fields (Zeeman effect regime) and "strong" fields (complete Paschen-Back regime) is more difficult to analyze since it requires a numerical diagonalization of the hamiltonian.

Socas-Navarro et al. (2004*a*) have pointed out that the determination of the magnetic field vector via the analysis of the observed polarization in the He I 10830 Å multiplet must be carried out considering the wavelength positions and the strengths of the Zeeman components in the incomplete Paschen-Back effect regime, since it may lead to emergent Stokes profiles significantly different from those corresponding to the linear Zeeman regime. Figure 8 shows the emergent Stokes profiles for the same model and magnetic field orientation of Fig. 7, but assuming that the strength of the field is 600 G. Unfortunately, with the only exception of Trujillo Bueno et al. (2002*a*), all of the research done with the He I 10830 Å multiplet has ignored this Paschen-Back effect. As it becomes obvious from Fig. 8, inversion codes based on the linear Zeeman effect theory (see, e.g., Lagg et al. 2004 and Solanki et al. 2003) may lead to a significant underestimation of the magnetic field strength. Fortunately, such codes can be easily improved via the use of the polynomial approximants provided by Socas-Navarro et al. (2005) for the calculation of polarization profiles in the He I 10830 Å multiplet.

2.6. The anti-level-crossings effect

In the absence of level crossings between the J-levels of the (L,S) term under consideration, or between the ensuing F-levels for the case of a hyperfine structured (HFS) multiplet like the Na I D_2 line, the theory of the Hanle effect predicts no modification of the emergent linear polarization with increasing strength of a magnetic field oriented parallel to the symmetry axis of the pumping radiation field (e.g., Stenflo 1994). For this reason, it is commonly believed that the scattering polarization is totally insensitive to vertical magnetic fields and that in solar limb observations we can only expect to measure the Hanle depolarization caused by inclined magnetic fields.

It is however important to note that this conventional view applies only to 'simple' lines like that of Sr I at $\lambda 4607$, but not to lines that result from transitions between spectral terms whose J-levels (or F-levels for the case of HFS multiplets) cross for a given range of magnetic field strengths. Thus, as shown in Fig. 2 of Trujillo Bueno et al. (2002*b*), the scattering polarization in the Na I D_2 line *increases* steadily with the magnetic strength, for *vertical* fields between about 10 and 100 gauss. This is caused by the quantum interferences, $\rho^2_Q(F,F')$, among different HFS levels in the $P_{3/2}$ upper level. In fact, in the 10–50 gauss range, numerous level crossings occur among

[6] A *coherent superposition* of two or more sublevels of a degenerate atomic level is a quantum mechanical state given by a linear combination of pure states of the atomic Hamiltonian.

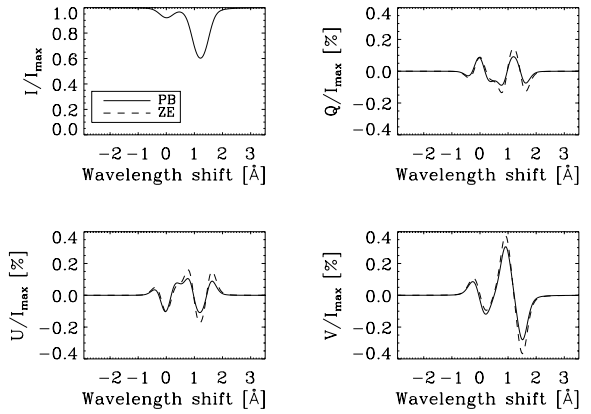

Figure 8. Model calculation of the emergent Stokes profiles of the He I *10830 Å multiplet at* $\mu = 1$ *assuming that a slab of helium atoms at a height of 3 arcseconds in the solar atmosphere is permeated by a deterministic magnetic field of 600 G with inclination* $\theta_B = 85°$ *and azimuth* $\chi_B = 65°$*. Only the influence of the Zeeman splitting is taken into account (i.e., atomic level polarization is disregarded in this illustrative example). Among several other differences, note that the calculation using the splittings and strengths of the linear Zeeman theory (dashed-line) produces Stokes profiles of larger amplitude than those corresponding to the incomplete Paschen-Back effect theory (solid line).*

the magnetic sublevels of the HFS levels with $F = 1, 2,$ and 3 of the $P_{3/2}$ upper-level of the Na I D_2 line. Interestingly, the theoretical prediction that vertical fields in the solar atmosphere produce magnetic enhancement of the scattering polarization in the Na I D_2 line (see Trujillo Bueno et al. 2002*b*), has been observationally confirmed by Stenflo et al. (2002) in a particularly interesting paper on Stokes vector imaging of the sodium doublet with a narrow-band universal filter.

Another very interesting example is shown in Fig. 9, which gives the emergent fractional linear polarization of the Ba II D_2 line in $90°$ scattering geometry for increasing values of the magnetic strength of the assumed *vertical* field. The solid line profile, which corresponds to the zero field case, is very similar to the observation that Stenflo & Keller (1997) obtained in a very quiet region close to the solar limb. As pointed out by Stenflo (1997), the central Q/I peak is due to the barium isotopes whithout hyperfine-structure (whose relative abundance amounts to 82%), while the two Q/I peaks in the wings are due to the odd isotopes (which have hyperfine-structure with nuclear spin $I = 3/2$ and a relative abundance of 18%). Therefore, our theoretical prediction is that in the D_2 line of Ba II we should also see enhancement of scattering polarization by a vertical field, but *only* at such wing positions because the required level crossings occur only between the F-levels of the $P_{3/2}$ upper level of the barium isotopes endowed of hyperfine structure. For the isotope 137 such level crossings occur between 50 and 500 G, approximately. As seen in Fig. 9, the central Q/I peak remains practically constant between 0 and 100 G, while as expected the two peaks in the wings increase with the strength of the vertical magnetic field. For magnetic fields stronger than 100 G the polarization is dominated by the transverse Zeeman effect, whose contribution is however not completely negligible for weaker fields and should always be calculated within the framework of the incomplete Paschen-Back effect theory (Belluzzi et al. 2006).

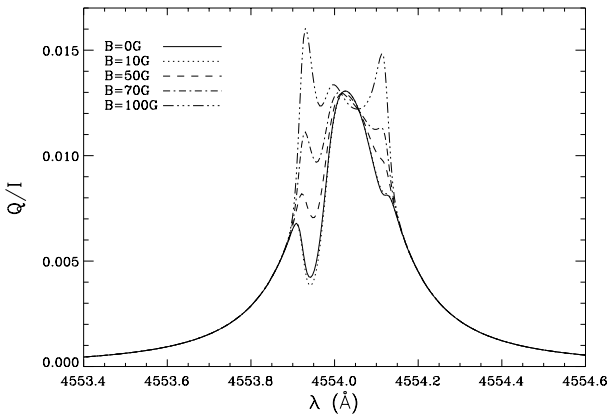

Figure 9. Theoretical calculation of the emergent linear polarization of the Ba II D_2 *line in* $90°$ *scattering geometry for increasing values of the assumed vertical magnetic field. The positive reference direction for Stokes Q is the parallel to the solar limb. From Belluzzi et al. (2006).*

The physical origin of this fascinating phenomenon is the so-called *anti-level-crossings effect*, which as pointed out by Bommier (1980) is related to the non-linear effect of the magnetic field on the energy levels in the transition from the Zeeman effect to the Paschen-Back effect.

In summary, the observation and modeling of the anti-level-crossings effect in suitably chosen spectral lines, such as the D_2 lines of Na I and Ba II, offers a very attractive diagnostic window for mapping the magnetic fields of the upper photosphere and chromosphere (e.g., via two-dimensional polarimetry with a tunable filter or with a Fabry-Perot interferometer).

3. TRANSFER OF POLARIZED RADIATION

In general, the physical interpretation of spectral line polarization requires calculating, for *multilevel* systems, the excitation and ionization state of chemical species of given abundance that is *consistent* with both the *intensity* and *polarization* of the radiation field generated within the (generally magnetized) plasma under consideration. This is a very involved *non-local* and *non-linear* radiative transfer (RT) problem which requires solving

the rate equations for the elements of the atomic density matrix (see below) and the Stokes-vector transfer equation for each of the allowed transitions in the multilevel model (e.g., Trujillo Bueno 2003*b*; Landi Degl'Innocenti & Landolfi 2004). Once such a selfconsistent excitation state is known along the line of sight, it is then straightforward to solve the transfer equation in order to obtain the emergent Stokes profiles to be compared with spectropolarimetric observations.

3.1. The Stokes-vector transfer equation

In the polarized case, instead of the standard RT equation for the specific intensity $I(x,\vec{\Omega})$ one has to solve, in general, the following *vectorial* transfer equation for the Stokes vector $\mathbf{I}(x,\vec{\Omega})=(I,Q,U,V)^{\dagger}$ ($\dagger$ = transpose):

$$\frac{d}{ds}\mathbf{I} = \mathbf{e} - \mathbf{K}\mathbf{I}, \tag{6}$$

where s measures the geometrical distance along the ray of direction $\vec{\Omega}$, $\mathbf{e}$ is the emission vector, and $\mathbf{K}$ the propagation matrix. The elements of the emission vector (that is, ϵ_I, ϵ_Q, ϵ_U, and ϵ_V) account for the contribution of the *spontaneous emission* process to the intensity and polarization that is generated at each spatial point by the physical mechanism under consideration. The propagation matrix $\mathbf{K}$ can be written as

$$\left(\begin{array}{cccc} \eta_I & 0 & 0 & 0 \\ 0 & \eta_I & 0 & 0 \\ 0 & 0 & \eta_I & 0 \\ 0 & 0 & 0 & \eta_I \end{array}\right) + \left(\begin{array}{cccc} 0 & \eta_Q & \eta_U & \eta_V \\ \eta_Q & 0 & 0 & 0 \\ \eta_U & 0 & 0 & 0 \\ \eta_V & 0 & 0 & 0 \end{array}\right)$$

$$+ \left(\begin{array}{cccc} 0 & 0 & 0 & 0 \\ 0 & 0 & \rho_V & -\rho_U \\ 0 & -\rho_V & 0 & \rho_Q \\ 0 & \rho_U & -\rho_Q & 0 \end{array}\right), \tag{7}$$

which helps to clarify that it has three contributions: absorption (the first matrix, $\mathbf{K_1}$, which is responsible for the attenuation of the radiation beam irrespective of its polarization state), dichroism (the second matrix, $\mathbf{K_2}$, which accounts for a selective absorption of the different polarization states), and dispersion (the third matrix, $\mathbf{K_3}$, which describes the dephasing of the different polarization states as the radiation beam propagates through the medium). Actually, the situation is more complicated (and interesting!) because in general the *propagation* matrix $\mathbf{K}=\mathbf{K}^{\rm A}-\mathbf{K}^{\rm S}$, where $\mathbf{K}^{\rm A}$ is the above-mentioned contribution resulting from transitions from the lower-level towards the upper-level, while $\mathbf{K}^{\rm S}$ is the contribution caused by the stimulated emission process. Thus, $\mathbf{K}^{\rm S}_1$ would be the amplification matrix (responsible for the amplification of the radiation beam irrespective of its polarization state), $\mathbf{K}^{\rm S}_2$ would be the dichroism matrix (responsible of a selective stimulated emission of different polarization states), and $\mathbf{K}^{\rm S}_3$ would be the corresponding dispersion matrix. Taking $\mathbf{K}^{\rm S}_2$ and $\mathbf{K}^{\rm S}_3$ into account may be of very great interest for new discoveries in the field of astronomical masers (e.g., Asensio Ramos et al. 2005).

The general expressions of the components of the emission vector and of the propagation matrix are very involved and will not be reproduced here (see Landi Degl'Innocenti & Landolfi 2004). They are given in terms of the ρ^K_Q elements of the upper and lower levels of the line transition under consideration and of lineshape profiles, whose dependence on the magnetic quantum numbers cannot be neglected when the Zeeman splittings are a significant fraction of the spectral line width. Such general expressions simplify considerably for several cases of practical interest. For instance, in the case of scattering line polarization in weakly magnetized regions of stellar atmospheres, ϵ_Q (η_Q) is a direction-dependent function of $\rho^2_Q({\rm up})$ ($\rho^2_Q({\rm low})$), with $Q=0,1,2$, while ϵ_U (η_U) is a different direction-dependent function of $\rho^2_Q({\rm up})$ ($\rho^2_Q({\rm low})$), but with $Q=1,2$. Thus, ϵ_Q and η_Q depend on both the population imbalances (ρ^2_0) and the quantum coherences (${\rm Re}(\rho^2_1)$, ${\rm Im}(\rho^2_1)$, ${\rm Re}(\rho^2_2)$, ${\rm Im}(\rho^2_2)$), while ϵ_U and η_U depend *only* on the coherences. Typically, in stellar atmospheres ϵ_I (η_I) is dominated by the overall population of the upper (lower) levels (i.e. by $\rho^0_0({\rm up})$ or $\rho^0_0({\rm low})$).

Fortunately, there are situations of practical interest for which the expressions of ϵ_Q and η_Q simplify considerably because the quantum coherences turn out to vanish (i.e. $\rho^2_1=\rho^2_2=0$). To this end, one has to choose the quantization axis of total angular momentum along the symmetry axis of the pumping radiation field (e.g., along the stellar radius vector for a one-dimensional stellar atmosphere model) and to assume that either the medium is unmagnetized or, for example, that the magnetic field is everywhere *microturbulent* and *isotropically distributed* with mixed magnetic polarities within very small scales (i.e., below the mean-free path of the line photons). Under these assumptions a very useful formula can be derived which can be applied to estimate the emergent fractional polarization at the core of a strong spectral line for an observation along the line of sight specified by $\mu=\cos\theta$ (Trujillo Bueno 2001; 2003*a*):[7]

$$Q/I \approx \frac{3}{2\sqrt{2}}(1-\mu^2)[\mathcal{W}\,\sigma^2_0({\rm up}) - \mathcal{Z}\,\sigma^2_0({\rm low})], \tag{8}$$

where $\sigma^2_0=\rho^2_0/\rho^0_0$ quantifies the *fractional atomic alignment* or *degree of population imbalance* of the upper or lower level of the line transition under consideration, while $\mathcal{W}$ and $\mathcal{Z}$ are simply numbers which depend on the quantum numbers of the transition (e.g., $\mathcal{W}=1$ and $\mathcal{Z}=0$ for a triplet-type transition with $J_l=0$ and $J_u=1$). Therefore, $\sigma^2_0(J)=0$ if the magnetic sublevels of the J-level turn out to be equally populated. Thus, the fractional linear polarization $Q/I=0$ if $\sigma^2_0=0$ in the

[7] In this expression, I have chosen the reference direction for $Q>0$ along the parallel to the stellar limb, as illustrated in Fig. 4.

upper and lower levels of the spectral line under consideration. In Eq. (8) the σ_0^2 values are those corresponding to the optical depth τ where $\tau/\mu \approx 1$ (which means $\tau = 0$ for a solar limb observation at $\mu = 0$). This expression for Q/I shows clearly that the observed fractional polarization produced by scattering processes in a given spectral line in general has two contributions: one from the fractional alignment of the upper-level ($\sigma_0^2(\mathrm{up})$) and an extra one from the fractional alignment of the lower level ($\sigma_0^2(\mathrm{low})$). The first contribution (caused exclusively by the emission events from the polarized upper level) is the only one that is normally taken into account. However, the second contribution (caused by the selective absorption resulting from the population imbalances of the lower level) plays the key role in producing the 'enigmatic' linear polarization signals that have been discovered recently in 'quiet' regions close to the solar limb, as well as in solar coronal filaments (see the reviews by Trujillo Bueno 1999, 2001, 2003*a*; see also Trujillo Bueno & Manso Sainz 2002).

3.2. The rate equations for the elements of the atomic density matrix

Since we are interested in the general Non-LTE case in which both collisions and radiative transitions can influence the excitation state, we need also to consider the master equation for the atomic density matrix (see Cohen-Tannoudji et al. 1992; Landi Degl'Innocenti & Landolfi 2004). Perhaps, the simplest and most famous example of this approach is that formulated by Einstein, who in 1917 introduced rate equations describing the effect of absorption, stimulated emission, and spontaneous emission processes between two levels of an atom immersed in a black-body radiation field. The situation is considerably more complex (and interesting!) in the present "polarized case" in which we have *atomic and light polarization* instead of simply overall population of the atomic levels and intensity. For instance, for a multilevel atom devoid of hyperfine structure and taking into account quantum coherences only between the sublevels pertaining to each J-level, the rate of change of the density matrix element $\rho^K_Q(J)$ *in the magnetic field reference system* reads

$$\frac{d}{dt}\rho^K_Q(J) \;=\; -2\pi \mathrm{i}\nu_L\, g_J\, Q\, \rho^K_Q(J) \qquad (9)$$

$$+\sum_{J_l}\sum_{K_l Q_l} \rho^{K_l}_{Q_l}(J_l)\, T_{\mathrm{A}}(J_l; K_l\, Q_l \;\rightarrow\; J; K\, Q)$$

$$+\sum_{J_u}\sum_{K_u Q_u} \rho^{K_u}_{Q_u}(J_u)\, T_{\mathrm{E}}(J_u; K_u\, Q_u \;\rightarrow\; J; K\, Q)$$

$$+\sum_{J_u}\sum_{K_u Q_u} \rho^{K_u}_{Q_u}(J_u)\, T_{\mathrm{S}}(J_u; K_u\, Q_u \;\rightarrow\; J; K\, Q)$$

$$-\sum_{K' Q'} \rho^{K'}_{Q'}(J)\, R_{\mathrm{A}}(J; K\, Q, K'\, Q' \;\rightarrow\; J_u)$$

$$-\sum_{K' Q'} \rho^{K'}_{Q'}(J)\, R_{\mathrm{E}}(J; K\, Q, K'\, Q' \;\rightarrow\; J_l)$$

$$-\sum_{K' Q'} \rho^{K'}_{Q'}(J)\, R_{\mathrm{S}}(J; K\, Q, K'\, Q' \;\rightarrow\; J_l)$$

$$-D^{(K)}(J)\, \rho^K_Q(J),$$

where $\nu_L = 1.3996 \times 10^6\, B$ is the Larmor frequency (with the magnetic field strength, B, in gauss). Besides including collisional rates like the last term on the rhs, which describes the local depolarization caused by elastic collisions, this equation accounts for radiative rates, both in the *transfer* rates due to absorption (T_{A}), spontaneous emission (T_{E}) and stimulated emission (T_{S}) *from* other levels, and on the *relaxation* rates due to absorption (R_{A}), spontaneous emission (R_{E}) and stimulated emission (R_{S}) *towards* other levels.[8] The explicit expressions for all these transfer and relaxation rates can be found in Landi Degl'Innocenti & Landolfi (2004). In particular, the transfer and relaxation rates due to absorption and to stimulated emission depend explicitly on a number of radiation field tensors which describe the symmetry properties of the radiation field (e.g., the *mean intensity* J^0_0 and the *anisotropy* J^2_0 defined in the caption of Fig. 4).

If the radiation field that illuminates the atomic or molecular system is given, one can then directly solve the statistical equilibrium equations (i.e., $\frac{d}{dt}\rho^K_Q(J) = 0$) in order to obtain the values of the ρ^K_Q elements. This directly solves *the optically thin problem* because, as mentioned above, the I, Q, U and V components of the emission vector are given in terms of the ρ^K_Q elements. However, in *optically thick media* we do not know a priori the radiation field within the medium. Therefore, in this more general case we are obliged to find the selfconsistent ρ^K_Q-values by solving iteratively the *non-local* and *non-linear* system of equations formed by the rate equations for the diagonal and non-diagonal elements of the atomic density matrix and the Stokes-vector transfer equations (see Trujillo Bueno & Manso Sainz 1999; Trujillo Bueno 2003*b*).

Finally, it is important to note that the astrophysical problem of the generation and transfer of polarized radiation is enormously simplified when the approximation of local thermodynamic equilibrium (LTE) is used, i.e., when one assumes that radiative transitions play no role in the populations of the energy levels[9]. As a result, there can be no atomic level polarization (i.e., neither population imbalances nor quantum interferences among the level's substates). In other words, the commonly made assumption of LTE excludes from the outset scattering line polarization and the Hanle effect. Moreover, it restricts the applicability of the Zeeman effect to spectral lines for which the LTE approximation turns out to be justified, and this depends on the particular stellar atmosphere model under consideration.

[8] For notational simplicity, I have not included the inelastic collisional rates, which are however taken into account in our radiative transfer simulations.

[9] The LTE approximation assumes that the level populations are only *locally* controled by collisions with an *isotropic* distribution of colliders.

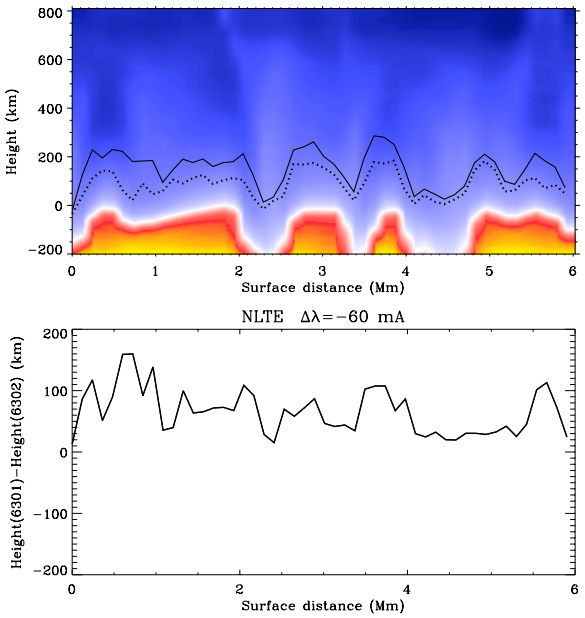

Figure 10. The top panel shows the horizontal fluctuation of the height where $\tau_{\rm line}(\Delta\lambda = -60\,{\rm m\AA}) = 1$ *in a realistic 3D hydrodynamical model of the solar photosphere, with the solid line corresponding to Fe* I $\lambda 6301.5$ *and the dotted line to* $\lambda 6302.5$*. Note that at many horizontal positions such heights coincide with atmospheric regions where the local gradients are very intense, but different for both spectral lines. The bottom panel shows the difference of such two heights in the solar model atmosphere.* $\Delta\lambda = \pm 60\,{\rm m\AA}$ *are typical wavelength positions from line center where internetwork Stokes V profiles use to have one of their lobes. The radiative transfer calculations have been carried out without assuming LTE. This figure is the result of an ongoing collaboration with Nataliya Shchukina.*

In conclusion, the diagnostic potential of spectropolarimetry is drastically reduced if polarization signatures resulting from 'Non-LTE effects' are disregarded. In order to open a truly empirical window on solar and stellar magnetism we must develop and apply remote sensing techniques based on both the Hanle and Zeeman effects.

4. APPLICATIONS IN SOLAR PHYSICS

This section shows some selected examples which illustrate how remote sensing techniques based on the Hanle and Zeeman effects are allowing us to investigate the hidden magnetism of the extended solar atmosphere. I consider only some aspects of the magnetism of the 'quiet' Sun.[10] In fact, this is the only relevant situation during the minimum of the solar magnetic activity cycle, in which no sunspots are seen on the solar surface. However, even during periods of strong magnetic activity most of the solar 'surface' is covered by the internetwork regions of the 'quiet' Sun. Moreover, there are many examples of solar plasma structures, such as spicules and coronal filaments, which play a key role with regard to the solar mass flux and/or the energy balance, and which owe their very existence to the presence of relatively weak magnetic fields.

4.1. A vast amount of hidden magnetic energy in the quiet solar photosphere

When one uses the Zeeman effect as a diagnostic tool of the 'quiet' regions of the solar photosphere one is able to obtain very useful information (e.g., Lin & Rimmele 1999; Sánchez Almeida & Lites 2000; Lites 2002; Socas-Navarro & Sánchez Almeida 2002; Domínguez Cerdeña et al. 2003a,b; Khomenko et al. 2003; Socas-Navarro et al. 2004b). The physical interpretation of the observed spectral line polarization is however puzzling, mainly because of the extreme inhomogeneity of the solar atmospheric plasma and the complexity of the spectral line formation problem in such a medium.

For instance, over the last few years the observational and theoretical evidence for small-scale mixture of weak and strong fields in the quiet Sun has increased considerably (e.g., Socas-Navarro & Sánchez Almeida 2003; Khomenko et al. 2003; Socas-Navarro & Lites 2004; Sánchez Almeida et al. 2003a,b; Cattaneo 1999; Cattaneo et al. 2003; Stein & Nordlund 2003, Vögler 2003), but also the controversy about the true abundance of kG fields in the internetwork regions of the quiet Sun (e.g., Domínguez Cerdeña et al. 2003a,b; Lites & Socas-Navarro 2004; Sánchez Almeida et al. 2004; de Wijn et al. 2005; Khomenko et al. 2005; Collados 2006). The uncertainty concerning the true value of the fraction of (internetwork) quiet Sun occupied by field strengths $B \geq 1$ kG will be drastically reduced after detailed investigations, similar to those carried out using the Fe I lines at $\lambda 6301.5$ and $\lambda 6302.5$ (e.g., Domínguez Cerdeña et al. 2003a,b; Sánchez Almeida et al. 2003b), are undertaken using instead the Fe I lines at $\lambda 5250.21$ and $\lambda 5247.05$, ideally in combination with *simultaneous* and *co-spatial* observations in the Fe I lines at $1.56\,\mu$m. One reason for this is that the Fe I lines at $\lambda 5250.21$ and $\lambda 5247.05$ are truly reliable for the application of the line-ratio technique for the Zeeman effect (Stenflo 1973), while this is not guaranteed for the $\lambda 6301.5$ and $\lambda 6302.5$ lines (Khomenko 2006), given that they do not have exactly the same absorption coefficient and the same behavior in the stratified and highly inhomogenous solar atmosphere (Shchukina & Trujillo Bueno 2001; see also Fig. 10).

Therefore, it is at present unclear whether or not the small-scale magnetic fields that we are able to 'see' via the Zeeman effect in the internetwork regions of the Sun are sufficiently strong and abundant so as to carry a truly

[10] The interested reader will find several excellent review papers on solar and stellar magnetism in the workshops edited by Sigwarth (2001), Mathys, Solanki & Wickramasinghe (2001), Trujillo Bueno & Sánchez Almeida (2003) and Casini & Lites (2006). See also the book of Schrijver & Zwaan (2000) on Solar and Stellar Magnetic Activity.

significant fraction of the unsigned magnetic flux and magnetic energy of the Sun. In this respect, it is of interest to mention that twelve years ago Keller et al. (1994) applied the magnetic line ratio technique to measurements of the Stokes V profiles of the Fe I lines at $\lambda 5250.21$ and $\lambda 5247.05$ and concluded that the strength of solar internetwork fields at the level of line formation is below 1 kG with high probability. As pointed out above, such type of observations should be repeated, but with higher spatial resolution and polarimetric sensitivity. For recent reviews with contrasting viewpoints on the magnetism of the very quiet Sun see Sánchez Almeida (2004); Collados (2006) and Khomenko (2006).

In the hydrodynamically controlled photosphere we expect to have highly tangled field lines with resulting mixed magnetic polarities on very small spatial scales, well below the current spatial resolution limit. For this reason, it is currently believed that via Zeeman effect diagnostics with the available instrumentation we are seeing only the "tip of the iceberg" of solar surface magnetism ($\sim 1\%$ of the photospheric volume according to Stenflo 1994, Domínguez Cerdeña et al. 2003a, and Khomenko et al. 2003). It is reasonable to expect that more locations with magnetic fields will be detected via the Zeeman effect when increasing the spatial resolution (see, however, Lites & Socas-Navarro 2004), and this is only one of the many scientific reasons for pursuing the development of space-borne telescopes like Solar-B [11], and ground-based solar telescopes like GREGOR [12] or the Advanced Technology Solar Telescope [13].

But, how to investigate in a reliable way the magnetism of the remaining $\sim 99\%$ of the volume of the 'quiet' solar atmosphere? How to obtain empirical information on the distribution of hidden, mixed-polarity magnetic fields at subresolution scales? Do such fields carry most of the unsigned magnetic flux and magnetic energy of the Sun? Or is this flux dominated by small-scale magnetic flux concentrations in the kG range as some recent Zeeman-effect investigations based on Fe I $\lambda 6301.5$ and Fe I $\lambda 6302.5$ seem to suggest (e.g. Domínguez Cerdeña et al. 2003a)? How is energy transported in a mixed magnetic-polarity environment? Can the ensuing magnetic field lines reach the solar chromosphere and corona? As discussed above, Zeeman effect polarization suffers from cancellation effects. Moreover, Zeeman polarization signals of weak tangled fields tend to have tiny amplitudes, well below the detection limit of the available instrumentation. Therefore, the investigation of magnetoconvection via spectropolarimetry cannot be done via the Zeeman effect *alone*. We need to complement our Zeeman diagnostic tools developed to interpret the observed *asymmetry* of Stokes profiles resulting from the co-existence of opposite magnetic polarities which do not cancel completely within the spatio-temporal resolution element (e.g., Socas-Navarro & Sánchez Almeida 2002) with new diagnostic techniques based on physical effects whose polarization signals do not suffer from cancellation effects.

The Hanle effect has the required diagnostic potential (Stenflo 1982), but the problem is how to apply it to obtain reliable information given that a Hanle-effect diagnostics relies on a comparison between the observed linear polarization and that calculated for the zero-field reference case. Shchukina & Trujillo Bueno (2003) have shown that the particular one-dimensional (1D) approach applied by Faurobert-Scholl et al. (1995; 2001) to the scattering polarization observed in the Sr I 4607 Å line yields artifitially low values for the strength of the "turbulent" field [14] -that is, between 20 and 10 G, as shown by the dashed lines of Fig. 3 in Shchukina & Trujillo Bueno (2003). This is because the scattering polarization amplitudes calculated by Faurobert-Scholl et al. (1995; 2001) for the zero-field reference case [i.e., $Q/I(B=0)$] was seriously underestimated due to their choice of the free parameters of 'classical' stellar spectroscopy (that is, micro- and macroturbulence for line broadening), which led to a sizable error in the value of the Hanle depolarization factor $\mathcal{D} = \frac{Q/I}{Q/I(B=0)}$ (where Q/I is the observed linear polarization amplitude). Note that the depolarization factor $\mathcal{D}$ is *similar* to the factor $\mathcal{H}^{(2)}$ given by Eq. (A-16) of Trujillo Bueno & Manso Sainz (1999), with $\mathcal{H}^{(2)} = 1$ for the zero-field reference case and $\mathcal{H}^{(2)} = 1/5$ for $B > B_{\rm satur}$ (where $B_{\rm satur} \approx 10 B_H$ is the saturation field of the Hanle effect for the spectral line under consideration). To understand why $\mathcal{D} \approx \mathcal{H}^{(2)}$ it suffices to note that Eq. (8) leads to the following Eddington-Barbier *approximation* for the emergent Q/I at the line-core of the Sr I 4607 Å line:

$$Q/I \approx \frac{3}{2\sqrt{2}}(1-\mu^2)\frac{\mathcal{H}^{(2)}}{1+\delta^{(2)}}\,A\,, \qquad (10)$$

where $\delta^{(2)}$ is the upper-level rate of (depolarizing) elastic collisions in units of the Einstein A_{ul} coefficient, and $A = J^2_0/J^0_0$ the degree of anisotropy of the spectral line radiation defined in the legend of Fig. 4. The particular 1D radiative transfer fitting approach of Faurobert-Scholl et al. (2001) gives $\mathcal{D} \approx 0.6$ (when using their THÉMIS Q/I measurements with the spectrograph's slit oriented at 45° with respect to the tangential direction to the observed solar limb), while it gives $\mathcal{D} \approx 0.8$ when using the accurate observational data shown in Fig. 11.

Trujillo Bueno et al. (2004) argue that reliable Hanle-effect diagnostics can be achieved by means of *three-dimensional* (3D) multilevel scattering polarization calculations in snapshots taken from realistic simulations of solar surface convection (see Stein & Nordlund 1998; Asplund et al. 2000). These radiation hydrodynamical simulations of the photospheric physical conditions are very convincing because spectral synthesis of a multitude of iron lines shows remarkable agreement with the observed spectral line profiles when the meteoritic iron

[11] http://science.msfc.nasa.gov/ssl/pad/solar/solar-b.stm
[12] http://gregor.kis.uni-freiburg.de/
[13] http://atst.nso.edu/

[14] By "turbulent" fields I simply mean magnetic fields hidden to Zeeman effect diagnostics with the available telescopes.

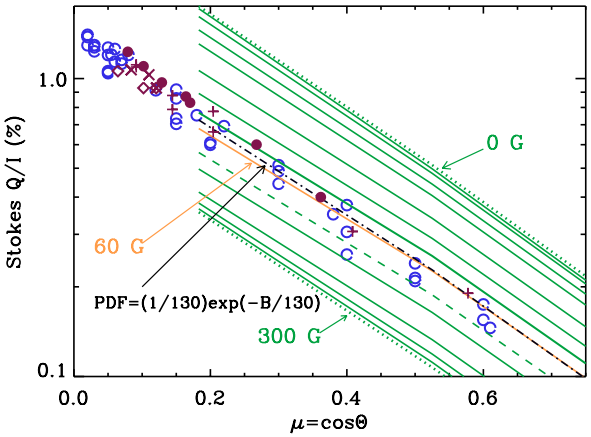

Figure 11. This figure shows the center-to-limb variation of the fractional linear polarization at the core of the Sr I *4607 Å line after substraction of the continuum polarization level. Open circles, various observations taken by Stenflo et al. (1997) during a minimum period of the solar cycle. The remaining symbols correspond to observations taken during the most recent maximum period of the solar cycle. Diamonds, observations obtained by Trujillo Bueno et al. (2001); crosses and 'plus' symbols, observations taken by Bommier & Molodij (2002) and by Bommier et al. (2005), respectively; filled circles, observations obtained in collaboration with M. Bianda. Coloured lines, the results of our 3D scattering polarization calculations in the presence of a volume-filling and single-valued microturbulent field (from top to bottom: 0, 5, 10, 15, 20, 30, 40, 50, 60, 80, 100, 150, 200, 250 and 300 gauss). Note that there is no evidence of a serious modulation of the observed Q/I with the solar magnetic activity cycle, and that the best average fit to the observations is obtained for 60 G. The black dashed-dotted line indicates the resulting Q/I amplitudes for the case of an exponential PDF with $\langle B\rangle = 130$ G. From Trujillo Bueno et al. (2004).*

abundance is chosen (Shchukina & Trujillo Bueno 2001). Therefore, we have used snapshots taken from such time-dependent hydrodynamical simulations in order to calculate the emergent Stokes profiles via 3D scattering polarization calculations using realistic multilevel atomic models. Our first target has been the Sr I line at 4607 Å, which is a normal triplet transition with $A_{ul}\approx 2\times 10^8 \mathrm{s}^{-1}$ and Landé factor $g_{J_u} = 1$. For the zero-field reference case we find that the spatially and temporally averaged emergent Stokes profiles give a Q/I that is substantially larger than the observed one, thus indicating the need for invoking magnetic depolarization. As it can be easily deduced from Fig. 11, we find $\mathcal{D}\approx 0.4$.

If our 3D result for $\mathcal{D}$ is correct, then any analysis based on $\mathcal{D}\approx 0.6$ (i.e., based on the above-mentioned 1D result) would imply a mean strength of the hidden field significantly smaller than what it actually is. For the same reason, if one uses a given distribution of magnetic field strengths, one would find more or less depolarization than $\mathcal{D}\approx 0.6$ depending on the mean field strength of the assumed distribution (see, e.g., the simplified analyses based on $\mathcal{D}\approx\mathcal{H}^{(2)}\approx 0.6$ carried out by Sánchez Almeida et al. 2003*a* and Stenflo & Holzreuter 2003). Obviously, the only way to end up with a solid conclusion concerning the unsigned magnetic flux and magnetic energy density carried by the *hidden field* is to use the correct depolarization factor $\mathcal{D}$.

We think that at present our 3D analysis of the scattering polarization in the Sr I 4607 Å line provides the most accurate estimation of $\mathcal{D}$, not only because our synthetic intensity profiles (which take into account the Doppler shifts of the convective flow velocities in the 3D model) are automatically in excellent agreement with the observed intensity profiles (i.e., *without* using the above-mentioned free parameters of classical stellar spectroscopy), but also because we were careful with the numerical calculation of the radiation field's anisotropy in the 3D hydrodynamical model. We solved the equations of Section 3 via the application of efficient radiative transfer methods (Trujillo Bueno 2003*b*), and using realistic collisional depolarizing rate values (Faurobert-Scholl et al. 1995), which turn out to be the largest rates among those found in the literature. Moreover, it is also of interest to mention that the recent work of Bommier et al. (2005) strongly supports our result for $\mathcal{D}$.

We can thus conclude that the depolarization required to fit the Q/I observations of the Sr I 4607 Å line is with high probability of magnetic origin[15]. We have assumed that the hidden field is microturbulent with mixed polarities at subresolution scales, which is a reasonable assumption because in the quiet regions of the solar photosphere Stokes $U\approx 0$ (see, e.g., Fig. 2). It is obvious that with one single spectral line we do not have enough information to constrain the *shape* of the PDF[16]. For this reason, we assumed the shape of the PDF, as done by others before us (e.g., Faurobert-Scholl et al. 1995; 2001) and by others after us (e.g., Domínguez Cerdeña et al. 2005). The key point is however to be conservative in the choice of the functional form of the PDF, in order to avoid exagerating the resulting mean strength of the 'turbulent' field. For this very reason, Trujillo Bueno et al. (2004) presented the results of their investigation for the following two PDFs: (a) $\mathrm{PDF}(B) = \delta(B - \langle B\rangle)$ and (b) $\mathrm{PDF}(B) = e^{-B/\langle B\rangle}/\langle B\rangle$, with $\langle B\rangle$ the mean field strength.

The idealized model corresponding to option (a) will clearly underestimate $\langle B\rangle$, but we found it interesting to compare the ensuing magnetic energy with that corresponding to the kG fields of the network patches. The

[15] We are currently investigating whether or not bound-free transitions make any significant depolarizing influence on the atomic alignment of the upper level of the Sr I 4607 Å line (cf., Trujillo Bueno 2003*a*). For the moment I point out that the largest bound-free cross sections are those corresponding to the triplet levels, while the upper level of the Sr I 4607 Å line is a singlet.

[16] To this end, a good choice could be the linearly polarized spectrum of Ti I, whose multiplet Nr. 42 offers the attractive possibility of applying a Hanle-effect line-ratio technique (Manso Sainz et al. 2004; see also Shchukina & Trujillo Bueno 2006).

much more realistic option (b) is suggested by numerical experiments of turbulent dynamos and magnetoconvection (e.g., Cattaneo 1999; Stein & Nordlund 2003; Vögler et al. 2003). The PDF shape of some of such numerical experiments tends instead to be a *stretched exponential* which, as a first approximation, can be fitted by a Voigt function whose tail extends further out into the kG range than an exponential. Therefore, by choosing an exponential PDF instead of a Voigt PDF (or instead of any other better fitting function) we guarantee that we are not exagerating our estimation of $\langle B \rangle$. For this more realistic case (b), we also found important to compare the ensuing magnetic energy with that corresponding to the kG fields of the network patches (Trujillo Bueno et al. 2004).

As seen in Fig. 11, for the standard case (a) of a single-valued microturbulent field we found that $\langle B \rangle \approx 60$ G leads to a notable agreement with the observed Q/I. Note that the strength of the 'turbulent' field required to explain the Q/I observations seems to decrease with height in the atmosphere, from the 70 gauss needed to explain the observations at $\mu = 0.6$ to the 50 gauss required to fit the observations at $\mu = 0.1$. This corresponds to an approximate height range of between 200 and 400 km above the solar 'surface' (as seen at continuum optical depth unity).

Concerning the case of an exponential PDF, we see in Fig. 11 that $\langle B \rangle \approx 130$ gauss yields a fairly good *averaged* fit to the observed fractional linear polarization. In this much more realistic case $E_m = \langle B^2 \rangle / 8\pi \approx 1300 \ \mathrm{erg\,cm^{-3}}$ (that is, $\sqrt{\langle B^2 \rangle} \approx 180$ G), which is about 20% of the averaged kinetic energy density produced by convective motions at a height of 200 km in the 3D photospheric model. As pointed out by Trujillo Bueno et al. (2004), for this case the total magnetic energy stored in the internetwork regions turns out to be larger than that corresponding to the kG fields of the network patches.

Domínguez Cerdeña et al. (2005) have recently arrived to similar conclusions by combining magnetic field strength measurements based on the Zeeman effect in the Fe I lines at $\lambda 6301.5$, $\lambda 6302.5$, $\lambda 15648$ and $\lambda 15652$ and the Hanle effect in the Sr I 4607 Å line. In my opinion, it is not surprising that they find similar results to those of Trujillo Bueno et al. (2004) because (1) the fraction of quiet Sun producing the Zeeman polarization signals was $\sim 1.5\%$, (2) they used our depolarization factor $\mathcal{D} = 0.4$ for the Sr I 4607 Å line, and (3) they imposed the reasonable constraint that the magnetic energy density has to be significantly smaller than the kinetic energy density of the granular motions.

It is also worthwhile to point out that in order to be able to fit the observed polarization amplitudes given in Fig. 11, we need to use all the microturbulent magnetic fields with strengths between 0 and 500 G (i.e., taken from our exponential distribution of field strengths characterized by $\langle B \rangle$=130 G). All such microturbulent fields together (i.e., those with strengths between 0 and 500 G) have a filling factor of 98%. The remaining magnetic fields of the exponential distribution, whose strengths are larger than 500 G, have a filling factor of only 2% and they do not make any significant contribution to the 'observed' Hanle depolarization. In other words, if we only take the fields with strengths between 0 and 400 G (whose filling factor is 95%) we do not depolarize sufficiently (i.e., we do not reach the Q/I amplitudes indicated by the black dashed-dotted line of Fig. 11).

Taking into account that most of the solar surface is occupied by the 'quiet' internetwork regions of mixed polarity fields, it is clear that the results of our 3D analysis of the scattering polarization observed in the Sr I 4607 Å line might have far-reaching implications in solar and stellar physics. The hot outer regions of the solar atmosphere (chromosphere and corona) radiate and expand, which takes energy. By far the largest energy losses stem from chromospheric radiation, with a total energy flux of $\sim 10^7 \ \mathrm{erg\ cm^{-2}\ s^{-1}}$. The magnetic energy density corresponding to the simplest (and most conservative) model with $\langle B \rangle \approx 60$ G is 140 $\mathrm{ergs\,cm^{-3}}$, which leads to an energy flux similar to the above-mentioned chromospheric energy losses when using either the typical value of $\sim 1 \ \mathrm{km\,s^{-1}}$ for the convective velocities or the Alfvén speed ($v_A = B/(4\pi\rho)^{1/2}$, with ρ the gas density). In reality, as pointed out above, the true magnetic energy density that at any given time during the solar cycle is stored in the quiet solar photosphere is very much larger than $140 \ \mathrm{erg\,cm^{-3}}$. For example, the magnetic energy density corresponding to the (still conservative) case of an exponential distribution of field strengths with $\langle B \rangle \approx 130$ G is 1300 $\mathrm{ergs\,cm^{-3}}$, which implies an energy flux 10 times larger than that corresponding to the chromospheric radiative energy losses. Only a relatively small fraction would thus suffice to balance the radiative energy losses of the solar outer atmosphere.

Finally, it is very important to mention that analysis of the Hanle effect in molecular lines, such as those of C_2 and MgH, indicates that the mean strength of the volume-filling microturbulent field required to explain the observed molecular scattering polarization amplitudes is much smaller than what is needed to explain the above-mentioned observations of the Sr I 4607 Å line (Trujillo Bueno 2003*a*; Trujillo Bueno et al. 2004; Asensio Ramos & Trujillo Bueno 2005). The resolution of this puzzling behavior was found when it was pointed out (Trujillo Bueno 2003*a*) that the observed scattering polarization in very weak spectral lines, such as those of molecules, is coming *mainly* from the upflowing regions of the "quiet" solar photosphere (see Fig. 2 of Trujillo Bueno et al. 2004). In other words, the joined analysis of the Hanle effect in C_2 lines and in the Sr I 4607 Å line suggests that the strength of the hidden field fluctuates at the spatial scales of the solar granulation pattern, with much stronger fields above the intergranular regions (Trujillo Bueno et al. 2004). Interestingly, we find that the distribution of magnetic field strengths *in the (intergranular) downflowing regions of the quiet solar photosphere* has to be such that it produces saturation

for the Hanle effect in the Sr I 4607 Å line there[17]. This constraint is needed because, only when we are close to Hanle-effect saturation in the downflowing plasma, the additional microturbulent field of the upflowing regions needed to fully explain the Q/I observations of the Sr I 4607 Å line turns out to be weak enough to satisfy the requirements of our analysis of the Hanle effect in molecular lines. One *illustrative* example of a distribution of microturbulent fields that satisfies such a constraint is the Maxwellian PDF used by Trujillo Bueno et al. (2004) *for the downflowing regions of the quiet solar photosphere*, which incorporates some pieces of the the information given by Zeeman-effect measurements (e.g., that in the quiet Sun we also have magnetic fields significantly stronger than $B_{\rm satur}\approx$200 G). Note that this illustrative PDF implies that the filling factor of kG fields is $\sim$2% of the downflowing volume -that is, it does not exclude the possibility (Domínguez Cerdeña et al. 2003a) of small-scale kG fields in the internetwork regions. We point out that with such a Maxwellian PDF *for the downflowing plasma* (which has its maximum value at 456 G!), most of the magnetic energy is carried by chaotic fields with strengths between the equipartition field values and $\sim$1 kG. The same conclusion would be reached with other (more realistic) examples of PDFs for the intergranular plasma (e.g., a Gaussian?), as far as they satisfy the constraint of producing saturation of the Hanle effect for the strontium line.

In summary, our combined analysis of the Hanle effect in molecular lines and in the Sr I 4607 Å line leads to the conclusion that there is a vast amount of hidden magnetic energy and (unsigned) magnetic flux in the inter-network regions of the 'quiet' solar photosphere, carried mainly by rather chaotic fields in the (intergranular) downflowing plasma with strengths between the equipartition field values and $\sim$1 kG (Trujillo Bueno et al. 2004). The presence of this hidden magnetic field in the quiet internetwork regions of the solar photosphere might have several important consequences for the overlying solar atmosphere, such as ubiquity of reconnecting current sheets and heating processes (e.g., Schrijver & Title 2003; Close et al. 2004).

4.2. Chromospheric magnetism and solar spicules

Let us now address the following question of how we could investigate the magnetism of the upper solar chromosphere. In my opinion, one attractive possibility is via spectropolarimetric observations of *solar spicules*. These features were described in 1877 by Father Secchi as jet-like, elongated structures in the solar atmosphere. Spicules are best seen when observing a few arcsec off the limb in various chromospheric emission lines, such as Hα or the lines of neutral helium at λ5876 and λ10830. It is commonly believed that most of the chromospheric emission in these lines comes from spicules, and that at

[17]As seen in Fig. 11, saturation for the simplest case of a single-valued field occurs for $B>B_{\rm satur}\approx$200 G.

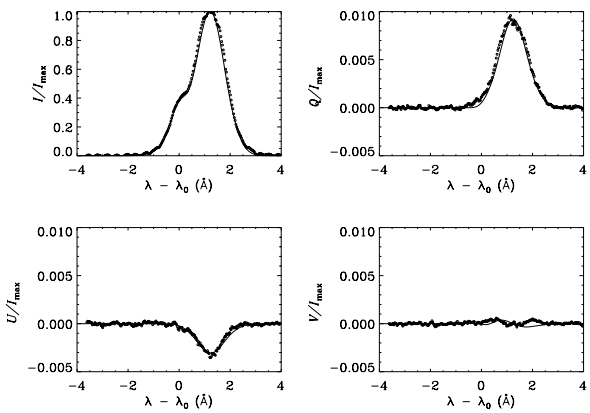

Figure 12. Open circles: observational example of Stokes profiles produced by (quiet-Sun) chromospheric spicules. The reference direction for Stokes Q is the parallel to the solar limb. The origin of the wavelength scale corresponds to the blue component of the He I 10830 Å multiplet. Solid line: optically thick theoretical modeling for a magnetic field strength $B = 10$ G, inclination $\theta_B = 37^\circ$ and azimuth $\chi_B = 173^\circ$. From Trujillo Bueno et al. (2005a).

heights exceeding 1500 km above the photosphere the solar chromosphere is mainly composed of spicular material. As reviewed by Beckers (1972), these 'geyser-like' plasma structures show upward velocities reaching 25 km s^{-1} lasting for some 5 min, but with a path that is frequently slanted with respect to the local vertical direction. After reaching a typical maximum height of 9000 km, the ejection stops and is followed by a fading of the spicule brightness or a return of the emitting material to the photosphere. Interestingly, in the upward-moving phase the spicule mass flux exceeds the mass loss of the solar corona through the solar wind by two orders of magnitude!

All theoretical models aimed at explaining the origin of spicules invoke magnetic field effects. What has really been lacking up to very recently are spectropolarimetric investigations to infer the strength and geometry of the magnetic field that is thought to channel the spicular motion (see Trujillo Bueno et al. 2005a; Socas-Navarro & Elmore 2005; López Ariste & Casini 2005).

Figure 12 shows an example of the full Stokes vector of the He I 1083 nm multiplet, which Trujillo Bueno et al. (2005a) observed with the Tenerife Infrared Polarimeter (TIP) attached to the Vacuum Tower Telescope (VTT) of the Observatorio del Teide (Tenerife). The spectrograph slit was located $\sim$2.5 arcsec off the limb and parallel to it, thus crossing the spicular material that we could see clearly in the slit-jaw H$_\alpha$ image. This spectropolarimetric observation is very encouraging, especially because of the detection of a non-zero Stokes-U profile. According to the theory of the Hanle effect, this Stokes-U profile is the observational signature of the presence of a weak magnetic field *inclined* with respect to the solar radius

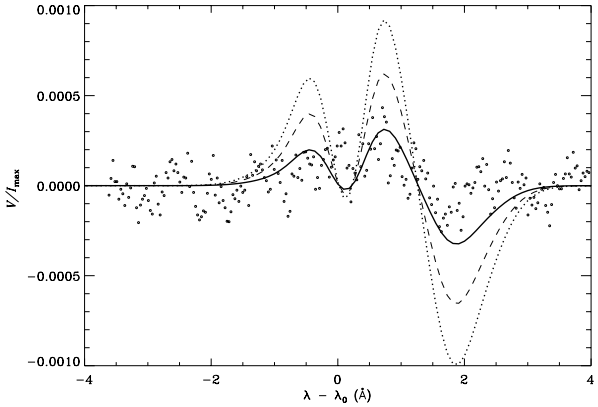

Figure 13. Open circles: the observed Stokes V profile at one of the spatial points in our observations of (quiet-Sun) chromospheric spicules. The origin of the wavelength scale corresponds to the blue component of the He I *10830 Å multiplet. The solid, dashed and dotted lines show theoretical Stokes V profiles for magnetic fields of 10 G, 15 G and 20 G, respectively, all of them with an inclination and azimuth that fits the observed linear polarization.*

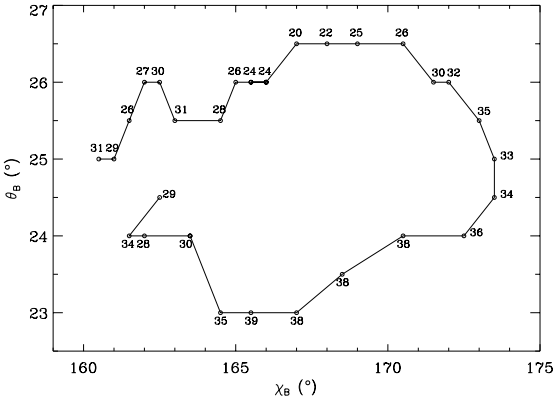

Figure 14. Inclination (θ_B), azimuth (χ_B), and strength (in gauss) of the magnetic field vector of a polar crown prominence, which was inferred from the observed polarization of the He I *10830 multiplet at consecutive spatial points along the spectrograph slit. From Merenda et al. (2006).*

vector through the observed point. Note that that the Stokes-V signal is at the noise level, suggesting that the field is weak, as clarified later in Fig. 13.

A best fit to the observations can be achieved via theoretical modeling of the Hanle and Zeeman effects (see Trujillo Bueno et al. 2005a). The example of Fig. 12 accounts for radiative transfer effects. As seen in this figure, our theoretical modeling of the observed Stokes profiles is notable. It suggests that in quiet regions the magnetic field that channels the spicular motions is of the order of 10 G and inclined by about 35° to the local solar vertical. Figure 13 reinforces our conclusion that the mean field strength along the line of sight of our spectropolarimetric observation of quiet-Sun spicules was not much larger than 10 G. Our empirical finding should be taken into account in future MHD simulations of quiet Sun spicules. For example, De Pontieu et al. (2004) assumed an inclined flux tube with 120 G in the low corona. Their MHD simulation aimed however at modeling the dynamic jets observed in *active region fibrils*, instead of the *spicules* of the quiet Sun.

4.3. The magnetic field that confines the plasma of solar prominences

Solar prominences are relatively cool and dense ribbons of plasma located tens of thousands of kilometers above the visible 'surface' of the Sun and embedded in the 10^6 K solar corona. They represent interesting physical systems where magnetic fields are interacting with plasma in subtle ways, where dense plasma is being supported against gravity and where thermal instabilities and/or continual magnetic flux emergence and reconnection processes might be creating the cool dense gas (e.g., the review by Priest 1989). By studying these objects in detail we can learn how such fundamental processes are likely to operate elsewhere in the Universe. On the other hand, the eruption of a prominence often produces a coronal mass ejection, which may have a dramatic influence on near-Earth space weather.

The Tenerife Infrared Polarimeter allows us to measure the four Stokes parameters with high degree of sensitivity in the near IR. Using this instrument attached to the German Vacuum Tower Telescope and modeling the observed spectral line polarization within the framework of the quantum theory of line formation, we are investigating the three-dimensional structure of the magnetic fields that confine the plasma of solar prominences (see also Casini et al. 2003). To this end, we have developed suitable inversion algorithms for deriving the magnetic field vector from the observed polarization in the He I 10830 multiplet. Figure 3 in the letter by Trujillo Bueno et al. (2002a) contrasts our theoretical modeling versus the observed Stokes profiles in one of the many prominences we have observed. Figure 14 shows that the magnetic field vector in a polar crown prominence that was located at the solar south pole is *rotating* around a fixed direction in space (given by $\theta_B \approx 25^\circ$ and $\chi_B \approx 168^\circ$) as we move along consecutive spatial points.

4.4. How to 'measure' the magnetic field of the solar transition region and corona?

The solar corona is a very effective emitter of Lyman α radiation (Gabriel et al. 1971). Such a radiation results from the resonance scattering of disk Lyman α photons by residual coronal neutral hydrogen (Gabriel 1971).

This conclusion has led some authors to propose the Hanle effect in the Lyman α line as a diagnostic of the strength and direction of coronal magnetic fields between approximately 1 and 3 solar radii from sun center (Bommier & Sahal-Bréchot 1982; Fineschi et al. 1992). Obviously, this refers to the 90° scattering case.

On the other hand, the intensity profiles of the hydrogen lines of the Lyman series have been measured on the solar disk by several instruments on board rockets and space telescopes (e.g., by the SUMER spectrometer on SOHO), showing that such lines are in emission at all positions and times and that they originate in the upper chromosphere and transition region (e.g., Warren et al. 1998). Therefore, it is of great interest to investigate the diagnostic potential of the Hanle effect in the hydrogen lines of the Lyman series for the forward scattering case (Casini & Trujillo Bueno 2006; in preparation).

Interestingly, the scattering polarization of the hydrogen lines of the Lyman series are sensitive (via the Hanle effect) to the typical magnetic strengths expected for the solar outer atmosphere (chromosphere, transition region and corona). According to Eq. (4), the critical magnetic fields of the hydrogen lines of the Lyman series are approximately the following:

$Ly_\alpha\,(1216\text{Å}) \rightarrow B_H = 50$ gauss

$Ly_\beta\,(1025\text{Å}) \rightarrow B_H = 20$ gauss

$Ly_\gamma\,(\ 972\text{Å}) \rightarrow B_H = 8$ gauss

$Ly_\delta\,(\ 950\text{Å}) \rightarrow B_H = 4$ gauss

$Ly_\epsilon\,(\ 937\text{Å}) \rightarrow B_H = 2$ gauss

Figure 15 shows a theoretical example of the linear polarization signal created by the Hanle effect of a horizontal magnetic field in the Lyman α line. This spectral line results from transitions between a lower term, $1s^2\mathrm{S}_{1/2}$ (which has a single level with $J = 1/2$), and an upper term, $2p^2\mathrm{P}_{1/2,3/2}$ (which has two levels with $J = 1/2$ and $J = 3/2$). We have taken into account not only the hyperfine structure, but also quantum interferences between the ensuing F-levels, even between those belonging to different J-levels within the same term. Although such refinements are not very important for the Lyman α line, they cannot in general be neglected for modeling the Hanle effect for other hydrogen lines.

In conclusion, as illustrated in Fig. 15, these forward scattering polarization signals offer a novel diagnostic tool for mapping the magnetic fields of the solar transition region and corona. Obviously, the required observations can be realized only from a UV/EUV spectropolarimeter on board of a space telescope.

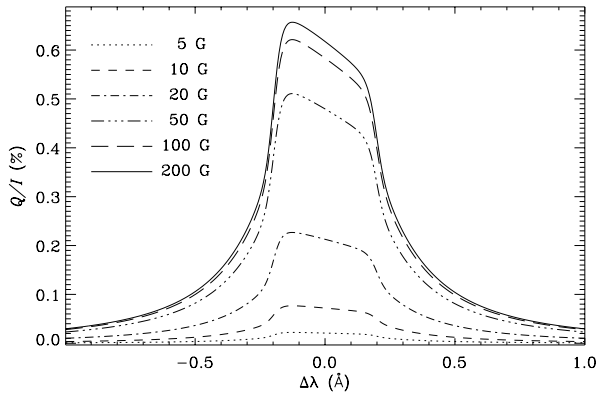

Figure 15. Theoretical estimate of the linear polarization created by the Hanle effect in the Lyman α line as a result of forward scattering processes in the presence of a horizontal magnetic field in the solar transition region. Note that the Q/I amplitude increases with the strength of the magnetic field, up to the Hanle-effect saturation field intensity ($\sim$ 200 gauss for the forward scattering case in the presence of a horizontal field). The calculations have been carried out assuming a slab of hydrogen atoms at a height of 3000 Km above the solar visible surface and neglecting the contribution of the center-to-limb variation of the Lyman α radiation on the anisotropy factor. From Trujillo Bueno et al. (2005b).

5. CONCLUDING REMARKS

Polarized light provides the most reliable source of information at our disposal for the remote sensing of astrophysical magnetic fields, including those on the Sun. However, in order to open a true empirical window on solar and stellar magnetism, we urgently need a high-sensitivity polarimeter in a space telescope and cleverly-designed ground-based telescopes optimized for spectropolarimetric observations.

I bear no doubt that *Quantum Spectropolarimetry* will be a revolutionary technique in 21^{st} century astrophysics. ESA should take advantage of the present European leadership in this field to open this new diagnostic window on the Universe.

ACKNOWLEDGMENTS

This work has benefited from finantial support through the project AYA2004-05792 of the Spanish Ministerio de Educación y Ciencia.

REFERENCES

Asensio Ramos, A., Landi Degl'Innocenti, E., Trujillo Bueno, J. 2005, ApJ, 625, 985

Asensio Ramos, A., Trujillo Bueno, J. 2005, ApJ Letters, 635, in press

Asplund, M., Nordlund, Å., Trampedach, R., Allende-Prieto, C., & Stein, R.F. 2000, A&A, 359, 729

Beckers, J.M. 1972, ARA&A, 10, 73

Belluzzi, L., Trujillo Bueno, J., & Landi Degl'Innocenti, E. 2006, in *Solar Polarization 4*, eds. R. Casini & B. Lites, B., ASP Conf. Series Vol. in press

Bommier, V., 1980, A&A, 87, 109

Bommier, V., Sahal-Bréchot, S. 1982, Solar Phys. 78, 157

Bommier, V., & Molodij, G. 2002, A&A, 381, 241

Bommier, V., Derouich, M., Landi Degl'Innocenti, E., Molodij, G., & Sahal-Bréchot, S. 2005, A&A, 432, 295

Bohr, N. 1924, Naturwissenschaften, 12, 1115

Born, M., & Wolf, E. 1994, *Principles of Optics*, Pergamon Press, Oxford

Casini, R., López Ariste, A., Tomczyk, S., Lites, B. W. 2003, ApJ, 598, L67

Casini, R., & Lites, B. (eds.) 2006, *Solar Polarization 4*, ASP Conf. Series Vol. in press

Cattaneo, F. 1999, ApJ, 515, L39

Cattaneo, F., Emonet, T., & Weiss, N. 2003, ApJ, 588, 1183

Close,R.M., Parnell,C.E., Longcope,D.W., & Priest,E.R. 2004, ApJ, 612, L81

Cohen-Tannoudji, C., Dupont-Roc, J., & Grynberg, G. 1992, Atom-Photon Interactions: Basic Processes and Applications, John Wiley & Sons

Collados, M. 2006, in Solar Polarization 4, eds. R. Casini & B. Lites, ASP Conf. Series Vol. in press

Collados, M., Trujillo Bueno, J., Asensio Ramos, A. 2003, in Solar Polarization 3, eds. J. Trujillo Bueno & J. Sánchez Almeida, ASP Conf. Series 307, 468

Condon, E.U., & Shortley, G.H. 1935, *The Theory of Atomic Spectra*, Cambridge University Press, Cambridge

De Pontieu, B., Erdélyi, R., & James, S. P. 2004, Nature, 430, 536

de Wijn, A.G., Rutten, R.J., Haverkamp, E.M., & Sütterlin, P. 2005, A&A, 441, 1183

Domínguez Cerdeña, I., Kneer, F. & Sánchez Almeida, J. 2003*a*, ApJ, 582, L55

Domínguez Cerdeña, I., Sánchez Almeida, J., & Kneer, F. 2003*b*, A&A, 407, 741

Domínguez Cerdeña, I., Sánchez Almeida, J., & Kneer, F. 2006, ApJ, 636, 496

Faurobert-Scholl, M., Feautrier, N., Machefert, F., Petrovay, K., & Spielfiedel, A. 1995, A&A, 298, 289

Faurobert-Scholl, M., Arnaud, J., Vigneau, J., & Frisch, H. 2001, A&A, 378, 627

Fineschi, S. et al. 1992, SPIE Vol. 1742, 423

Gabriel, A. H. 1971, Solar Phys., 21, 392

Gabriel, A. H., et al. 1971, ApJ, 169, 595

Gandorfer, A. 2000, *The Second Solar Spectrum*, Vol. 1: 4625 Å to 6995 Å ISBN 3 7281 2764 7 (Zürich: vdf)

Gandorfer, A. 2002, *The Second Solar Spectrum*, Vol. 2: 3910 Å to 4630 Å ISBN 3 7281 2855 4 (Zürich: vdf)

Gandorfer, A. 2005, *The Second Solar Spectrum*, Vol. 3: 3160 Å to 3915 Å ISBN 3 7281 3018 4 (Zürich: vdf)

Hanle, W. 1924, Z. Phys., 30, 93

Happer, W. 1972, Rev. Mod. Phys., 44, 169

Heisenberg, W. 1925, Z. Phys., 31, 617

Kastler, A. 1950, J. de Physique, 11, 255

Keller, C.U., Deubner, F.L., Egger, U., Fleck, B., & Povel, H.P. 1994, A&A, 286, 626

Khomenko, E. 2006, in Solar MHD: Theory and Observations - a high spatial resolution perspective" , eds. J. Leibacher, H. Uitenbroek & R. F. Stein, ASP Conf. Series, Vol. in press

Khomenko, E.V., Collados, M., Solanki, S., Lagg, A., & Trujillo Bueno, J. 2003, A&A, 408, 1115

Khomenko, E.V., Shelyag, S., Solanki, S., & Vögler, A. 2005, A&A, 442, 1059

Lagg, A., Woch, J., Krupp, N., Solanki, S. 2004, A&A, 414, 1109

Landi Degl'Innocenti, E., Landolfi, M. 2004, *Polarization in Spectral Lines*, Kluwer Academic Publishers

Lin, H., & Rimmele, T. 1999, ApJ, 514, 448

Lites, B., 2002, ApJ, 573, 431

Lites, B., & Socas-Navarro, H., ApJ, 613, 600

López Ariste, A., & Casini, R. 2005, A&A, 436, 325

Manso Sainz, R., Trujillo Bueno, J. 2003, Phys. Rev. Letters, 91, 111102-1

Manso Sainz, R., Landi Degl'Innocenti, E., & Trujillo Bueno, J. 2004, ApJ, 614, L89

Mathys, G., Solanki, S.K., & Wickramasinghe, D. (eds.) 2001, *Magnetic Fields Across the H-R Diagram*, ASP Conf. Series, Vol. 248

Merenda, L., Trujillo Bueno, J., Landi Degl'Innocenti, E., Collados, M. 2006, ApJ, in press

Mitchell, A.C.G., & Zemansky, M.W. 1934, *Resonance Radiation and Excited Atoms*, Cambridge University Press

Moruzzi, G., Strumia, F. (eds.) 1991, *The Hanle Effect and Level-Crossing Spectroscopy*, New York: Plenum

Priest, E. 1989, in Dynamics and Structure of Quiescent Solar Prominences, ed. E. Priest, Kluwer.

Sánchez Almeida, J. 2004, in The Solar-B Mission and the Forefront of Solar Physics, eds. T. Sakurai & T. Sekii, ASP Conf. Series 325, 115

Sánchez Almeida, J., & Lites, B. 2000, ApJ, 532, 1215

Sánchez Almeida, J., Emonet, T., & Cattaneo, F. 2003*a*, ApJ, 585, 536

Sánchez Almeida, J., Domínguez Cerdeña, I., & Kneer, F. 2003*b*, ApJ, 597, L177

Sánchez Almeida, J., Márquez, I., Bonet, J.A., Domínguez Cerdeña, I., & Muller, R. 2004, ApJ, 609, L91

Schrijver, C. J., & Zwaan, C. 2000, Solar and Stellar Magnetic Activity, Cambridge University Press

Schrijver, C. J., & Title, A. 2003, ApJ, 597, L165

Shchukina, N., & Trujillo Bueno, J. 2001, ApJ, 550, 970

Shchukina, N., & Trujillo Bueno, J. 2003, in Solar Polarization 3, eds. J. Trujillo Bueno & J. Sánchez Almeida, ASP Conf. Series Vol. 307, 336

Shchukina, N., & Trujillo Bueno, J. 2006, in Solar Polarization 4, eds. R. Casini & B. Lites, ASP Conf. Series Vol. in press

Sigwarth, M. (ed.) 2001, *Advanced Solar Polarimetry: Theory, Observation and Instrumentation*, ASP Conf. Series, Vol. 236

Socas-Navarro, H., & Sánchez Almeida, J. 2002, ApJ, 565, 1323

Socas-Navarro, H., & Sánchez Almeida, J. 2003, ApJ, 593, 581

Socas-Navarro, H., & Lites, B. 2004, ApJ, 616, 587

Socas-Navarro, H., & Elmore, D. 2005, ApJ, 619, L195

Socas-Navarro, H., Trujillo Bueno, J., & Landi Degl'Innocenti, E. 2004*a*, ApJ, 612, 1175

Socas-Navarro, H., Martínez Pillet, V., & Lites, B. 2004*b*, ApJ, 611, 1139

Socas-Navarro, H., Trujillo Bueno, J., & Landi Degl'Innocenti, E. 2005, ApJ Supplement Series, 160, 312

Solanki, S. K., Lagg, A., Woch, J., Krupp, N., Collados, M. 2003, Nature, 425, 692

Stein, R.F., & Nordlund, Å. 1998, ApJ, 499, 914

Stein, R.F., & Nordlund, Å. 2003, in *IAU Symposium 210: Modeling of Stellar Atmospheres*, eds. N. E. Piskunov, W. W. Weiss, D. F. Gray, ASP Conf. Series Vol. 210, 169

Stenflo, J.O. 1973, Solar Phys., 32, 41

Stenflo, J.O. 1982, Solar Phys., 80, 209

Stenflo, J.O. 1994, *Solar Magnetic Fields: Polarized Radiation Diagnostics*, Kluwer Academic Publishers

Stenflo, J.O., 1997, A&A, 324, 344

Stenflo, J.O. 2002, in *Astrophysical Spectropolarimetry*, J. Trujillo Bueno, F. Moreno-Insertis & F. Sánchez (eds.), Cambridge University Press, 55

Stenflo, J.O., & Keller, C. 1997, A&A, 321, 927

Stenflo, J.O., Bianda, M., Keller, C. U., & Solanki, S.K. 1997, A&A, 322, 985

Stenflo, J.O., Keller, C., & Gandorfer, A. 2000, A&A, 355, 789

Stenflo, J.O., Gandorfer, A., Holzreuter, A., Gisler, D., Keller, C., & Bianda, M. 2002, A&A, 389, 314

Stenflo, J.O., & Holzreuter, R. 2003, in Current Theoretical Models and Future High Resolution Solar Observations: Preparing for ATST, ASP Conference Series, Vol. 286, 169

Trujillo Bueno, J. 1999, *Towards the Modelling of the Second Solar Spectrum*, in Solar Polarization, eds. K. N. Nagendra and J. O. Stenflo, Kluwer Academic Publishers, 73

Trujillo Bueno, J. 2001, *Atomic Polarization and the Hanle Effect*, in Advanced Solar Polarimetry: Theory, Observation and Instrumentation, ed. M. Sigwarth, ASP Conf. Series 236, 161

Trujillo Bueno, J. 2003*a*, *New Diagnostic Windows on the Weak Magnetism of the Solar Atmosphere*, in Solar Polarization 3, eds. J. Trujillo Bueno & J. Sánchez Almeida, ASP Conf. Series 307, 407

Trujillo Bueno, J. 2003*b*, *The Generation and Transfer of Polarized Radiation in Stellar Atmospheres*, in Stellar Atmosphere Modeling, eds. I. Hubeny, D. Mihalas and K. Werner, ASP Conf. Series 288, 551

Trujillo Bueno, J., Landi Degl'Innocenti, E. 1997, ApJ Letters, 482, L183

Trujillo Bueno, J. & Manso Sainz, R. 1999, ApJ, 516, 436

Trujillo Bueno, J. & Manso Sainz, R. 2002, *Remote Sensing of Chromospheric Magnetic Fields via the Hanle and Zeeman Effects*, Il Nuovo Cimento, Vol. 25 C, No. 5-6, 783

Trujillo Bueno, J., Collados, M., Paletou, F. & Molodij, G. 2001, in Advanced Solar Polarimetry: Theory, Observation and Instrumentation, ed. M. Sigwarth, ASP Conf. Series 236, 141

Trujillo Bueno, J., Landi Degl'Innocenti, E., Collados, M., Merenda, L. & Manso Sainz, R. 2002*a*, Nature, 415, 403

Trujillo Bueno, J., Casini, R., Landolfi, M., Landi Degl'Innocenti, E. 2002*b*, ApJ Letters, 566, L53

Trujillo Bueno, J., & Sánchez Almeida, J. (eds.) 2003, *Solar Polarization 3*, ASP Conf. Series Vol. 307

Trujillo Bueno, J., Shchukina, N., Asensio Ramos, A. 2004, Nature, 430, 326

Trujillo Bueno, J., Merenda, L., Centeno, R., Collados, M., Landi Degl'Innocenti, E. 2005*a*, ApJ Letters, 619, L191

Trujillo Bueno, J., Landi Degl'Innocenti, E., Casini, R., & Martínez Pillet, V. 2005*b*, *The Scientific Case for Spectropolarimetry from Space*, in Proc. 39*th* ESLAB Symposium, Noordwijk, 19-21 April 2005, eds. F. Favata & A. Gimenez, ESA Publications Division, in press

Vögler, A. 2003, PhD thesis, Göttingen University, Göttingen

Warren, H.P., Mariska, J.T., Wilhelm, K. 1998, ApJS, 119, 105